



VisionNet: An efficient vision transformer-based hybrid adaptive networks for eye cancer detection with enhanced cheetah optimizer

Akshaya B^{*}, Sakthivel P

Department of Electronics and Communication Engineering, College of Engineering Guindy, Anna University, Chennai, Tamil Nadu 600025, India



ARTICLE INFO

Keywords:
 Eye Tumor Detection
 Vision Transformer-based Hybrid Adaptive Networks
 Residual Attention Network
 MobileNetV2
 Enhanced Cheetah Optimizer

ABSTRACT

Due to the uncontrolled growth of cells, the detection of eye cancer is important in the healthcare sector. Thus, it affects the interior parts of the eye or extra-ocular, affecting the exterior parts of the eye. However, treating the malignant affected area earlier may be advisable in the case of eye cancer. Eye cancer is detected using several deep-learning techniques. These techniques have certain challenges like high computational cost and also require high time for processing. Therefore, it is necessary to overcome these issues using conventional methods for eye cancer detection. Initially, the images for eye cancer detection are taken from internet resources with a total of 140 images. These gathered images are given as input to the eye cancer detection network. Here, the Vision Transformer-based Hybrid Adaptive Networks (ViT-HAN) is used to detect eye cancer with a fused combination of Residual Attention Network (RAN) and MobileNetV2. Further, the RAN and MobileNetV2 parameters are tuned using the Enhanced Cheetah Optimizer (ECO) algorithm. Hence, the developed eye cancer detection model secures an effectively higher performance rate than the conventional eye cancer detection techniques. The accuracy of the proposed model was 97 %, with a false positive rate of 3.0 % and a false negative rate of 3.0 %. Throughout the empirical outcomes, the developed model performs superior to existing techniques. These results emphasize that proposed frameworks could greatly enhance clinical procedures by improving patient outcomes and diagnostic accuracy in ocular oncology.

1. Introduction

Eye cancer is caused by a dangerous tumor known as melanoma. The initial stage of melanoma is mostly found in the skin or on the eye coating. It frequently grows on the tissues at the middle layer of the eyeball [1]. The uvea is located at the core part of the eyeball and the iris is present inside the uvea. These tumors on the iris show various side effects and signs [2] and some of the signs are light spots on the region of the iris, differences in size and slight variations in the vision [3]. The human iris plays a vital role in the optical system for managing light rays obtained by the retina in the eyeball. If the tumor grows inside the iris, then it may affect the eyesight [4]. The iris tumor occurs when the light spot on the iris changes size and enlarges. It is also known as Glaucoma. This disease damages the optic nerve in the eye and causes loss of sight [5]. Near Glaucoma, pupil deformation and evolution of cataracts present below the lymph and the blood vessels on the lymph signifies that the tumors are cancerous [6]. The tumors that don't show any symptoms are more dangerous than other tumors that could be examined only by

an eye-care specialist. Hence, huge biomedical machines were used to detect iris cancer [7].

In medical image processing techniques, conventional methods are used to detect tumor tissue to provide details about the shape analysis that helps to detect the changes in the volume of the lymph and also to provide an accurate treatment plan to eradicate the tumor. It is one of the important techniques in tumor tissue detection [8]. Image segmentation and image processing approaches are commonly used techniques to solve medical issues related to the lungs and brain, gross tumor volume and optimization of CT dose [9]. Based on this consideration, medical image processing techniques are also used to develop a specific solution for patients with iris tumors [10]. Although many studies have been conducted on ophthalmology-related problems, only a few automatic systems have been developed to detect tumor cells on the iris and other related tissues that change over time [11]. However, several experiments were performed to examine other characteristics related to the eye. A 3D structure of the eye is introduced to imitate the thermal effect in the tumor where Pennes' Bioheat Transfer Equation (PBHTE) is

* Corresponding author at: Department of Electronics and Communication Engineering, College of Engineering Guindy, Anna University, Chennai, Tamil Nadu 600025, India.

E-mail address: akshayacsc95@gmail.com (A. B.).

used to determine the temperature in the tumor cells [12]. Popular techniques of image segmentation are generally used for tumor detection which is mostly applied only to the segmentation of brain tumors. Because iris segmentation is challenging due to the occurrence of eyelashes that cause iris occlusion and pupil dilation that occurs due to diverse light illumination along with certain uncontrollable factors on eyes and applying those techniques for iris segmentation is not addressed in the image processing literature. Despite the structural similarity of human eyes, automatic segmentation techniques based on images suffer from different issues. However, this slight difference is important in optimum high-precision planning. [13].

High-precision planning and radiation are necessary for retinal tumor therapy to protect the non-affected healthy anatomical structure and eye power [14]. The Gullstrand eye model is commonly used in many planning tools. This eye model eliminates individual deflections and depicts the eye in a spherical shape which can be seen in the myopic eye [15]. Imaging techniques like Computed Tomography (CT) and Magnetic Resonance Imaging (MRI) provide more accurate information related to the eye [16]. Therefore, it is highly useful for making the decision. To develop a data-driven model of an eye, the digital images should be segmented based on their similar structure, which is followed by the reconstruction of three-dimensional forms [17]. Yet, the usage of high-resolution images leads to larger datasets. Therefore, time-consuming supervised segmentation techniques are used to reduce the compliance between the medical users and clinical interest in automatic segmentation might be increased. Here, a novel Eye Tumor Detection Model (ETDM) is developed.

1.1. Prevalence of eye cancer

The most dangerous condition that can affect anyone over the age of 40 worldwide is eye cancer. For eye cancer to be effectively treated, early detection and treatment are important. The survival rate is primarily derived from 2020 data, which shows that 46,680 new cases are being assessed globally. According to the Age-Standardized Rate (ASR), there were 0.49 cases of eye cancer per 100,000 people. When these survey reports were collected, the results for Sub-Saharan Africa showed that the region had a higher incidence of eye cancer, with an ASR rate of 4.06 [18]. The prevalence of eye cancer in both males and females is higher in Western Europe than in Northern Europe and other Asian regions. Furthermore, GLOBOCAN and CI5 are used to represent the universal incidence and death rate of eye tumors.

Recently, India has seen a significant enlarge in the cancer rate. In the healthcare sector, patient information is obtained via the Electronic Medical Records (EMRs) system to assist with treatment choices and medical decision-making [19]. In India, the prevalence of eye cancer is quite low with the majority of cases occurring in adults and the remaining cases in children. It anticipates that there were 1486 new cases of eye cancer in 2013, the year with the greatest incidence [20]. As a result, 54 % of men and 46 % of women are reported to have eye cancer collectively. With the aid of the American Cancer Society, 3360 new cases of eye cancer and 410 deaths have been estimated for 2022. The American Cancer Society estimated that tumors of the orbit and eye, primarily melanomas will be found in 1,780 cases of men and 1,540 cases of women by 2024. Additionally, 560 deaths from orbital and ocular cancer were estimated affecting 260 men and 300 women [21].

1.2. Artificial intelligence (AI) in ocular oncology

The detection and diagnosis of eye tumors are being greatly improved by AI, which uses novel techniques such as deep learning to achieve remarkable results with high accuracy. AI systems have demonstrated remarkable potential in the highly accurate and precise analysis of medical pictures, especially based on deep learning. AI algorithms can rapidly process and interpret enormous volumes of data from several imaging modalities, including magnetic resonance imaging

(MRI), optical coherence tomography (OCT) and fundus photography that human examiners may overlook, which improves prognosis and allows for earlier discovery.

Using Google's DeepMind AI, which has been trained on millions of retinal scans to identify over 50 different eye disorders, including eye tumors, is another significant example [22]. This method has proven to be as accurate as a highly trained ophthalmologist, which has greatly increased the rates of early detection, reduced the risk of misdiagnosis and enabled prompt treatments.

Another important application of deep learning techniques has been in the development of automated tools for histopathology image analysis [23]. In humans, uveal melanoma is the most common primary intraocular tumor and can be reliably diagnosed as benign or malignant using a deep learning technique which demonstrated the promise of AI in pathological diagnoses with its excellent accuracy rate, which having been trained on thousands of digitized tissue specimens.

AI-driven technologies are being incorporated into telemedicine platforms in real-world applications to enable remote diagnosis and consultations. For instance, an AI system may evaluate images given by remote clinics and offer medical professionals real-time diagnostic assistance, guaranteeing prompt referral and care. Furthermore, by monitoring the progression of a disease and evaluating individual risk factors, AI's predictive analytics capabilities can provide individualized treatment strategies in clinical ophthalmology [24]. In addition to this, AI not only increases the precision and efficacy of detecting eye cancer but also offers wider accessibility to these cutting-edge diagnostic methods to a wider population, including people who reside in underprivileged areas.

These developments show how AI, in particular, deep learning is revolutionizing the detection of eye cancer through its technologies that improve diagnostic accuracy, reduce the likelihood of human error and promote early intervention.

1.3. Conventional methods used by clinicians to detect eye cancer

Several conventional techniques are extensively available and widely used in clinical practice since they have been developed over time and are frequently an aspect of standard diagnostic therapies giving better clinical decisions for the detection of eye cancer. Automatic techniques provide reliable and effective screening thus improving early detection and treatment of eye cancer whereas conventional methods depend on human interpretation which may be error-prone. To detect eye cancer, physicians use several kinds of conventional methods from standard vision tests to advanced specialized diagnostic procedures.

- Visual test [25]: The first step in detecting eye cancer is typically a comprehensive examination of the eye. This could entail examining the retina, optic nerve in the eye and other tissues with specialized tools such as an ophthalmoscope.
- Slit lamp test [26]: A brightly lighted microscope known as a slit lamp allows a physician to perform a detailed examination of an eye. This can aid in the detection of anomalies in the eye such as abnormalities in the iris or pupil's size, shape or irregular development on the exterior part of the eye.
- Fundoscopy/Ophthalmoscopy [27]: This method involves viewing structures inside the eye including the retina, optic nerve and blood vessels with a specialized device called an ophthalmoscope. Using ophthalmoscopy, physicians can identify anomalies including tumors, additional signs of ocular malignancy and retinal detachments.
- Diagnostic imaging [28]: The eye and surrounding structures can be assessed with imaging techniques including ultrasonography, Magnetic Resonance Imaging (MRI), Computed Tomography (CT) scans, Optical Coherence Tomography (OCT), Indocyanine Green Angiogram (ICG) and Fluorescein Angiography (FA) which aid in the detection of tumors by determining the size and location of their growth.

- Tumor biopsies [29]: This can assist with determining the type and grade of tumor and confirm its presence.
- Genetic analysis [30]: When an inherited predisposition to eye cancer is suspected, genetic testing may be carried out to identify certain mutations related to specific forms of ocular tumors.

The major contributions of this developed model are given below.

- To develop a new ETDM using advanced methods to detect the tumor cells in the eye at an earlier stage to protect the patient's eye from the risk of losing their vision caused by the tumor cells. The detection of eye cancer can benefit a wide range of real-time healthcare industries.
- To propose an advanced technique called ViT-HAN by embedding RAN and MobileNetV2 for detecting the tumor cells in the eye where the parameters from the embedded model are optimized by the developed ECO to enhance the effectiveness of the model. Moreover, the ViT-HAN model aids in training the network model to provide better convergence and faster training performance in less time.
- To implement an improved tuning algorithm named ECO by enhancing specific features from the traditional CO algorithm and tuning the parameters such as "hidden neuron count, epoch count and steps per epoch" in both RAN and MobileNetV2 to improve the performance in terms of "accuracy, False Positive Rate (FPR), False Negative Rate (FNR)" in the proposed model. Therefore, the ECO algorithm can tune the complex parameters in challenging network structures.
- To compare the developed model with other classifiers and algorithms using various types of performance metrics to assess the model's effectiveness.

The implemented eye tumor detection framework is given below. The second section lists the advancements and drawbacks of the traditional models. The third part includes a brief overview of the proposed model. The development phase of the hybrid network for the eye cancer detection model is discussed in the fourth section. The detailed information about the developed ECO algorithm used to achieve better efficiency is described in the 5th section. The sixth section discusses the model's implementation and results while the seventh section includes the conclusion of the developed model.

2. Literature survey

2.1. Related works

In 2023, Zhong et al. [31] developed a markerless Beam's Eye View (BEV) algorithm using a deformable registration learning network to detect tumors from Megavolt (MV) images along with deformation and occlusion. The VoxelMorph model was trained on these datasets. At the same time, different images of lung tumors were collected to produce accurate motion data of tumors. The accuracy of this system was evaluated by using error tracking and image similarity. The image registration with non-rigid deformation and loss range could be handled by the tracking algorithm. Thus, a strong marker-less tumor tracking algorithm was developed to deal with partial and multi-modal data in addition to low-quality image processing.

In 2022, Fernando et al. [32] developed an effective approach using Convolutional Neural Networks (CNNs) to identify visual impairments along with a case study of Uveal Melanoma (UM). In existing models, UM was evaluated by using different methods such as adaptive neuro-fuzzy systems, neural networks and fuzzy systems by focusing on features using several computational techniques. The outcome from this model was compared with other computational algorithms for UM detection and the model had high accuracy, sensitivity and precision.

In 2021, Goswami et al. [33] proposed an adaptive method to detect eye cancer. This method selected the dataset that contained eye images

of untreated and treated mice. To perform automatic recognition and segmentation of eye images, four deep learning techniques were used to detect the difference between cancer affected region and the healthy retina, which is also used to segment the 3D form of visual tumor. The developed model's sensitivity analysis was compared with existing adaptive methods using measures such as reliability, speed and accuracy. U-Net with VGG-16 was used to treat the malign tumor and benign tumors can be treated using U-Net with Inception. The most and least sensitive performances were determined by the loss value and Root Mean Square Error (RMSE). Depending on training data, the performance of the system was improved. Segmented OCT-angiography data was used to determine the volume of the neo-vascularization. This analysis of the model's performance showed that the photodynamic imaging-assisted technique for tumor treatment causes tumor cells to proliferate quickly into the formation of a cyst that changes tumors into their benign stage. A specific system to detect the type and characteristics of a tumor was determined using an experimental equation.

In 2020, Cardoso et al. [34] developed an effective model to detect a choroidal melanoma tumor that has been identified at the rear side of the eye and could develop into metastasis. External Beam Radiotherapy (teletherapy) was the commonly used therapy to detect tumor cells in the advanced stage near the retina and protect the victim's eye. The main aim of this proposed method was to implement software to evaluate the eye throughout the treatment phase, to highlight the dislocation that could affect the exterior part of the target and to examine the eye with an automatic eye simulator. Increased accuracy and system reproducibility were obtained by this methodology.

In 2018, Ouabida et al. [35] developed an effective and automatic method to segment iris tumors and detect their related areas that were changing according to time. The network's primary goal was to evaluate various approaches that could be applied to segment the iris tumor. In the developed model, the VanderLugt Correlator (VLC) method was used in the segmentation process of eye tumors. Next, a one-pixel cluster depicting tumor tissue was created using the K-means clustering technique by treating the iris region. This system was aware of center initialization and distance measures. To overcome these issues, an approach based on proportional probability was developed for the center initialization of the cluster and a study was performed to detect the effects of several distance measures.

In 2016, Dimililer et al. [36] developed an image analysis system to detect eye tumors. In this developed model, tumor cells were extracted and highlighted on the original image by using several image-processing techniques. The median filtering was used to select the images. The image's background was separated and it was added to the original image resulting in the tumor-affected area or a brighter area of interest. Based on the outcomes achieved by the system, the model developed using image fusion can detect the tumor in the eye. Based on the effectiveness of detecting eye cancer, the results were assessed with the findings of existing systems.

In 2009, Ooi et al. [37] proposed a three-dimensional boundary element system to analyze the thermal impacts on the human eye based on the distribution of visual temperature. There were various thermal effects associated with each part of the eye. Cancer cells were also found among these eye parts. The thermal effects may cause tumor cells that were generated by the increased heat pressure and high perfusion rate in the blood vessels. The PBHTE was used to balance the temperature in a consistent state. Laplace's formula was used to resolve the temperature of normal tissues in the eye. The corneal surface temperature was calculated by dividing the surface boundaries into all eye regions to form triangular elements of the eye model.

Kunz et al. [38] developed an eye tumor detection model in 2004 with the aid of a database including eye models to better utilize the data provided with the MR image. Using an improved face detection technique, comparable features between the original image with the reference image are defined. The reference eye model was created by applying the minimized Mahalanobis distance, one of the similarity

Table 1

Advancements and limitations of classical ETDM.

Author [citation]	Methodology	Features	Challenges
Zhong <i>et al.</i> [31]	Markless tumor tracking algorithm	It effectively resolves the tracking errors attained in the evaluation.	It minimizes the tumor tracking speed and also shows little variations in accuracy when increasing the thickness of slices for larger targets.
Fernando <i>et al.</i> [32]	VGG and ResNet	It effectively minimizes the bias in the input images. It easily attains the high dimensional features that are independent of human intervention.	It does not produce stable performance when validating with huge datasets and requires more time for validating with small datasets.
Goswami <i>et al.</i> [33]	U-Net	It easily handles high-resolution input and provides accurate outcomes. It effectively minimizes the distortion rate by preserving the image structure.	It did not address the class imbalance issue. It requires additional time to identify a threshold value.
Cardoso <i>et al.</i> [34]	Eye position monitoring algorithm	It offers a high sampling rate with accuracy.	It is expensive to implement and needs more memory.
Ouabida <i>et al.</i> [35]	K-means Clustering	It provides the outcome with a high-resolution rate. It offers a high accuracy rate in detecting tumors. It has a good flexibility rate.	Its performance degrades over time and it is highly prone to errors when analyzing at high dimensional areas.
Dimililer <i>et al.</i> [36]	Median filtering	It offers a high robustness rate to the system. It identifies the abnormalities accurately in minimal time.	It is highly expensive and also complicated to validate.
Ooiet <i>et al.</i> [37]	Laplace's technique	It is easy to implement and also easily validates complex variables like time-domain functions.	It needs more time to analyze the input images.
Kunz <i>et al.</i> [38]	Gabor filtering	It identifies the textural features accurately. The overall tumor classification accuracy is improved effectively.	It needs more time to detect the tumor.
Fernando <i>et al.</i> [39]	VGG16 and ResNet	It effectively resolves the overfitting issues. It delivers a high accuracy rate in tumor classification.	VGG16 requires more time to train the images.
Kumar <i>et al.</i> [40]	ResNet and AlexNet	It achieved a high classification rate by employing multiple thresholds. It improves convergence speed and decreases the volume of labeled data necessary for training.	It requires additional time to determine the threshold value.
Junaid <i>et al.</i> [41]	Alexnet and ResNet-50	It successfully attains a high rate of accuracy. It effectively captures intricate patterns using the deep feature fusion approach.	It requires high computational resources.

metrics that are computed between the classified image and reference image, following a feature vector with a high dimension was generated using a trained dataset.

In 2022, Fernando *et al.* [39], the authors have developed the CNN model to detect ocular abnormalities for eye cancer classification. Additionally, various computing techniques such as the fuzzy system, adaptive model and neural network model were implemented and assessed to enhance performance. Additionally, by employing a transfer learning mechanism, the generated model's accuracy rate has increased outperforming its reliable performance. Furthermore, two methods were applied to reduce the bias in the dataset: one that used the Navier-Stokes method to eliminate light spots in the eye and the other that used the Gabor filter to perform data augmentation.

A method based on deep learning for processing text and image data was developed in 2023 by Kumar *et al.* [40]. The study was primarily centered on the CNN model for retinoblastoma tumor and non-tumor classification. To categorize cancerous regions, the ResNet and AlexNet models were used. The developed methods were more effective in differentiating between cancerous and normal tissues. The systematic approach that has been developed could offer an adaptable framework for the premature recognition of cancerous cells in the eye.

In 2023, Junaid *et al.* [41] developed an automated model for detecting retinal eye disease using Optical Coherence Tomography (OCT) images. For deep feature extraction, the ResNet-50 and AlexNet models were used. To reduce duplicate features, an ensemble entropy-based Ant Colony System (ACS) and Principal Component Analysis (PCA) selection process was employed. The publicly available datasets were used for the retinal eye disease whereas the various baseline methods were used to provide better outcomes. The most effective outcomes were obtained because of the deep future fusion approach and hybrid method of selection. Yet, the computational complexity of the model fails to provide effective outcomes. Parameter optimization has been not performed in this approach since it easily falls into the local minima problems.

This research work adapts the novel mechanism to effectively detect

eye cancer using the ECO algorithm's optimization technique to fine-tune the system's parameters and improve overall performance. As a result, the optimization algorithm solves the complex optimization issues and enhances the performance in terms of computational complexity. The resultant analysis provides better performance when compared to existing techniques.

2.2. Problem statement

Tumors grown in the tissues around the eye structure are known as ocular melanomas. It is more challenging for medical professionals to choose appropriate images for the evaluation because the tumors are identified inaccurately. Several advancements and risk effects presented in the conventional eye cancer detection models are presented in Table 1. The most important contributions comparing the related work are listed:

- In traditional methods, the detection of eye cancer becomes the challenging factor whereas the detection may not be accurate. In this research work, the detection model is performed using the hybridized approach which helps clinicians to detect eye cancer effectively.
- The overfitting issue in the existing techniques occurs during validation with a huge amount of data. Since the developed model can sequentially manage the data, it helps to enhance the system's performance and eliminates the overfitting issue using the transformer model.
- Certainly inaccurate detection results are emerging due to the higher negative measure which affects the performance of the system. However, the resulting analysis is carried out to show how effectively the constructed model lowers the negative measures.
- The training of the single network model for the ocular cancer detection framework is ineffective in comparison with existing techniques. The implementation of the hybrid adaptive network is the main focus of our research. To attain precise and accurate results,

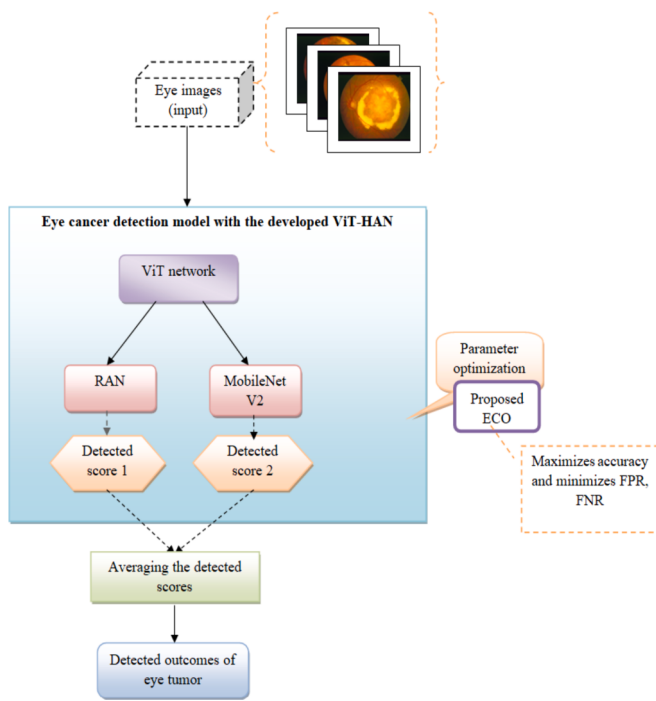


Fig. 1. Diagrammatic view of developed ETDM with hybrid adaptive networks.

the detected score from the RAN and MobileNetV2 model is averaged.

From [Table 1](#), the challenges mentioned are important to resolve several risk effects presented by conventional eye cancer detection methods.

3. Developing adaptive concepts on hybrid networks termed as hybrid adaptive networks using enhanced cheetah optimizer

3.1. Overall architecture of the implemented eye cancer detection model

Eye cancer is the uncontrolled development of tumor cells in the eye. A prevalent kind of eye tumor is melanoma. Different cells in the eyes are impacted by various types of tumors. People diagnosed with eye tumors may experience vision impairment and encounter several challenges. Imaging methods such as MRI scans provide a detailed view of soft tissues in the body, utilizing radio waves and strong magnets rather than X-rays. The accurate detection of eye tumors depends on the ability to observe ocular structures in detail, which can be made feasible by this type of imaging. However, for reliable and efficient tumor detection, an automatic approach is required because of the volume and complexity of MRI data. This results in the application of AI methods, which are highly accurate in detecting the existence of eye tumors by analyzing MRI data. Early detection and improved patient outcomes can be achieved by using AI algorithms that are trained to identify patterns associated with tumors. So, an automatic way of detecting the eye tumor is required, which leads to using deep learning techniques. Deep learning techniques provide effective results for eye tumor detection. However, the key challenge is to analyze the differences in gene expression [\[42\]](#) for detecting different types of eye tumors using machine learning approaches. Deep learning models are used in the detection system as a result of these limitations. Deep learning is capable of accurately detecting or segmenting eye tumors in less time. The deep-CNN [\[43\]](#) algorithm is the key method in iris image processing to detect the iris tumor, yet this method has poor anti-noise ability in the detection of tumors from the images. Convolution structures with different depths have a significant effect on the results. In tumor detection, CNN

configuration is better than other deep learning techniques. Since CNN provides better configuration, we use MobileNetV2, a variant of CNN and RAN [\[44\]](#) in the developed model to increase the performance of the system. A diagrammatic view of the developed ETDM with hybrid adaptive networks is shown in [Fig. 1](#).

The ETDM is developed to identify the tumor cells in the eye. Early detection of eye cancer is necessary to protect the patient's eye from several risk effects caused due to tumors. The eye images are collected from online sources which are mentioned in [section 4.1](#).

The early detection of eye cancer is aided by the AI algorithms; RAN and MobileNetV2, which can be trained to detect abnormalities and patterns in ocular imaging data. The collected images are given to the Hybrid Adaptive Networks (HAN) to detect the tumor cells in the eye. HAN is a combination of RAN and MobileNetV2. The major aim of RAN is to advance the performance of the framework and MobileNetV2 is used to produce faster detection results. The detected scores 1 and 2 (output values from both networks) are obtained from RAN and MobileNetV2. The average between the detected scores is taken as the final-detected outcome. The parameters of both RAN and MobileNetV2 are optimized by the developed ECO algorithm. Here, the parameters like "hidden neuron count, epoch count, and steps per epoch" in both RAN and MobileNetV2 are optimized by improved ECO. The developed ECO strategies increase the accuracy and decrease the FNR and FPR.

3.2. Conventional CO

CO algorithm [\[45\]](#) is a powerful tuning algorithm that imitates the hunting approaches of specific cheetahs. This algorithm uses three important strategies: the searching phase, the sitting and waiting stage and the attacking prey phase. At the time of searching for the prey and if the prey has been identified by a cheetah, then it will wait for the prey to get closer to it, which is then followed by the attacking mode. This attacking mode is used to reach its energy limits. After hunting the prey, the cheetah goes to its resting position and then again starts its new hunting. Cheetah populations were developed in many different orderings. Each cheetah's possible hunting ordering is considered equal to the solution for the difficulty. It is assumed that the most excellent position determines the best solution for the problem.

Searching strategy: A cheetah selects its prey by scanning the surroundings and searches based on the predator's behavior and environmental conditions. The arithmetical form of the searching phase is shown in Eq. [\(1\)](#).

$$A_{c,y}^{a+1} = A_{c,y}^a + R_{c,y}^{-1} \cdot \alpha_{c,y}^a \quad (1)$$

In Eq. [\(1\)](#), the phrase $A_{c,y}^a$ indicates the cheetah's current order and the term $A_{c,y}^{a+1}$ indicates the new order of the cheetah c at the time a . The randomization parameter is obtained by the inverse of the distributed random number denoted as $R_{c,y}^{-1}$. The term $\alpha_{c,y}^a$ defines the random step length and it is expressed in Eq. [\(2\)](#)

$$\alpha_{c,y}^a = 0.001 \times \frac{c}{C} \times (U_y - V_y) \quad (2)$$

here, the terms U_y represent the upper limit, the phrase V_y represents the lower limit of the variable y , and the phrase C indicates the maximum time for hunting. Here, the value 0.001 is fixed based on step length $\alpha_{c,y}^a$. For the other members of the cheetah group, the random step length $\alpha_{c,y}^a$ is indicated as the distance between the cheetah c and a random cheetah l in a group. It is arithmetically shown in Eq. [\(3\)](#).

$$\alpha_{c,y}^a = 0.001 \times \frac{c}{C} \times (A_{c,y}^a - A_{l,y}^a) \quad (3)$$

here, the term $A_{c,y}^a$ and $A_{l,y}^a$ represents the locations of the current cheetah and the random cheetah, respectively.

Sitting-and-waiting strategy: Cheetahs are fast predators. When

they chase prey, their speed and flexibility necessitate more energy. As a result, there cannot be an extensive period between the attack and the chase. Thus, waiting until their prey approaches them before engaging in battle is the most important mechanism. Here, the cheetah stays in the same position in the waiting mode to attack its prey which is expressed as shown in Eq. (4)

$$A_{c,y}^{a+1} = A_{c,y}^a \quad (4)$$

Attacking strategy: At the right time, the cheetah attacks its prey. Velocity and flexibility are two crucial factors that cheetahs exploit during their attacks. Cheetahs attack at the maximum speed, so cheetahs must get close to their prey in a very short time. At this stage, the prey notices the attack of the cheetah and starts running. The cheetah uses its considerable elasticity to hold the target in an unstable position. Attacks can happen individually or in groups. At the time of individual attack, the position of the cheetah varies based on the prey's location. This could be done effectively in a group attack, depending on the target and the location of other group members. This strategy is explained mathematically in Eq. (5)

$$A_{c,y}^{a+1} = A_{B,y}^a + R_{c,y}^z \cdot \beta_{c,y}^a \quad (5)$$

here, the phrase $A_{B,y}^a$ refers to the prey's position, which is the optimization factor that represents the prey's quick changes. Also, the term $R_{c,y}^z$ is an arbitrarily selected value from a usual allocation, which is determined for estimating the sharp turns made by the cheetah at the time of capturing mode. This is represented in Eq. (6).

$$R_{c,y}^z = |R_{c,y}|^{\exp(R_{c,y}/2)} \sin 2\pi R_{c,y} \quad (6)$$

In Eq. (6), the term $\sin 2\pi R_{c,y}$ indicates the turning angles of the cheetahs. The turning factor is represented as $\beta_{c,y}^a$ which is computed between the cheetah's position $A_{c,y}^a$ and the leader's position $A_{l,y}^a$ during the capturing models shown in Eq. (7)

$$\beta_{c,y}^a = A_{l,y}^a - A_{c,y}^a \quad (7)$$

Strategy selection method: The right approach in the CO algorithm is arbitrarily chosen. Let r_1 and r_2 be two arbitrary numbers from a consistent distribution. The sit-and-wait approach is selected if $(r_1 \geq r_2)$ is satisfied, then the sit-and-wait approach will be performed or else either the attacking strategy or searching strategy will be performed based on a random value F that is mathematically expressed in Eq. (8).

$$F = e^{2\left(1 - \frac{c}{C}\right)} (2R - 1) \quad (8)$$

here, the term C represents the maximum time for hunting and c represents the present hunting time. The random value R ranges between $[0, 1]$. The attacking and searching strategies have been defined with the condition of $(F \geq r_3)$ where the term r_3 represents the random variable that is ranged between $[0, 3]$. The pseudocode of conventional CO is presented in algorithm 1.

Algorithm 1: Conventional CO

```

Initialize the population (Cheetahs) $A_x(x = 1, 2, \dots, k)$ 
Evaluate the fitness function
For  $xc \leftarrow 1$ 
While ( $I \leq MaxI$ ) do
    Select  $cm(2 \leq cm \leq cn)$  members of cheetahs randomly.
    For  $x \in cm$  do
        Estimate the nearest member  $c$ 
        For every arrangement,  $y \in \{1, 2, \dots, S\}$  do
            Evaluate  $R, R^z, \alpha, \beta$  and  $F$ 
             $r1, r2 \leftarrow$  selected random numbers
            if ( $r1 \geq r2$ ) then
                If ( $F \geq r3$ ) then
                    Calculate the latest member position of the cheetah  $x$  using Eq. (5)
                Else
                    Calculate the latest member position of the cheetah  $x$  using Eq. (1)
            End
            Update the solution of the leader and member  $c$ 
        End for
         $I \leftarrow I + 1$ 
        Achieve the optimal solution
    End

```

(continued on next column)

(continued)

Algorithm 1: Conventional CO

```

Calculate the latest member position of the cheetah  $x$  using Eq. (1)
End
Else
    Calculate the latest member position of the cheetah  $x$  using Eq. (4)
End
End
Update the solution of the leader and member  $c$ 
End for
 $I \leftarrow I + 1$ 
Obtain the best solution
End

```

3.3. Developed ECO-based parameter optimization

The developed ECO is used for tuning the parameters of the developed model and the features such as “hidden neuron count, epoch count and steps per epoch” for both RAN and MobileNetV2 are optimized to augment the performance and efficiency of the implemented model. CO was chosen for this proposed model because it solves a wide range of complex issues. Yet, it has certain challenges whereas the result achieved by CO has lower efficacy as compared to other approaches. Hence, an improved strategy is developed and termed as ECO. In the developed ECO, the random number $r3$ is updated based on the concept of the objective function using Eq. (9), whereas, in conventional CO, it is taken randomly in the range of $[0, 3]$.

$$r3 = \frac{B_{sol}^c}{(W_{sol}^c \times M_{sol}^c)} \quad (9)$$

In Eq. (9), the variable $r3$ represents the updated random variable, B_{sol}^c is the “best fitness” value of the cheetah, W_{sol}^c is the “worst fitness” value of the cheetah and M_{sol}^c is the “mean fitness” value. The pseudocode for the developed ECO is presented in algorithm 2.

Algorithm 2: Proposed ECO

```

Initialize the population (Cheetahs) $A_x(x = 1, 2, \dots, k)$ 
Evaluate the fitness function
For  $xc \leftarrow 1$ 
While ( $I \leq MaxI$ ) do
    Select  $cm(2 \leq cm \leq cn)$  members of cheetahs randomly.
    For  $x \in cm$  do
        Estimate the nearest member  $c$ 
        For every arrangement,  $y \in \{1, 2, \dots, S\}$  do
            Evaluate  $R, R^z, \alpha, \beta$  and  $F$ 
             $r1, r2 \leftarrow$  selected random numbers
            if ( $r1 \geq r2$ ) then
                A random number  $r3$  is updated adaptively using Eq. (9)
                If ( $F \geq r3$ ) then
                    Calculate the latest member position of the cheetah  $x$  using Eq. (5)
                Else
                    Calculate the latest member position of the cheetah  $x$  using Eq. (1)
                End
            End
            Calculate the latest member position of the cheetah  $x$  utilizing Eq. (4)
            End
            Update the solution of the leader and member  $c$ 
        End for
         $I \leftarrow I + 1$ 
        Achieve the optimal solution
    End

```

The flow diagram of ECO's optimization technique is shown in Fig. 2.

4. Developing a hybrid network using residual attention network and MobileNetV2

4.1. Dataset collection

Dataset 1: In this research work, to achieve reliable results for the

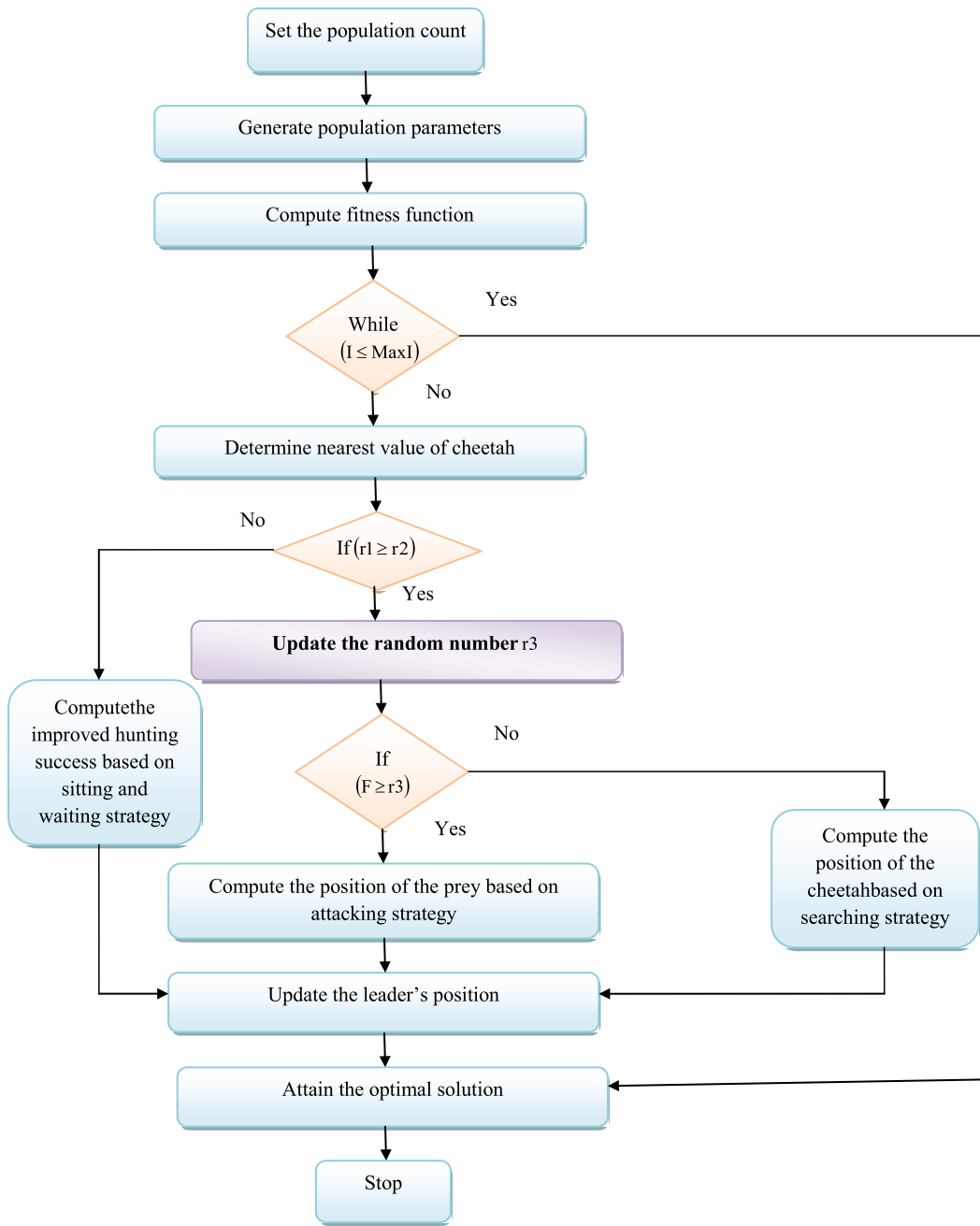


Fig. 2. Flow diagram of the proposed ECO.

efficient detection of eye cancer, the implementation is carried out using benchmark datasets for the ETDM model. The developed ETDM uses a retinoblastoma dataset [40].

Fig. 3 depicts the sample images from experimental datasets 1 and 2.

Dataset 2: This dataset is obtained from the standard source [46]. This dataset can include diverse samples which can be beneficial for the detection process. This may additionally improve the model's robustness by enhancing the diversity of data used for training.

Equitable benchmarking and comparison of various models and algorithms are made feasible by the utilization of two datasets, which provide diversified samples that are advantageous for the detection process. By evaluating models on different datasets, researchers and practitioners can assess their performance under various scenarios and would make informed decisions about model selection and deployment.

4.2. RAN

The RAN [44] is structured by stacking several attention modules. A single attention block is separated into a trunk branch and a mask branch. The trunk section processes the feature data and it is capable of attaining any state-of-the-art model architecture. This network uses ResNeXt, Inception and a Pre-Activation Residual unit as the key parts to develop an attention module in the RAN framework. The result obtained from the trunk section is represented as $T(i)$ with input data i , the mask section uses top-down and bottom-up approaches to achieve the equivalent mask size $M(i)$ and weights of the resultant characteristics $T(i)$. The feedback attention process and fast-feed-forward process were simulated by bottom-up and top-down approaches. Output mask is employed to function as the control gate for the trunk branch neurons, which is similar to the process of highway network [47] which is one of the deep learning networks. The outcome of the attention module N is

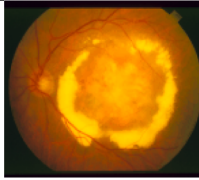
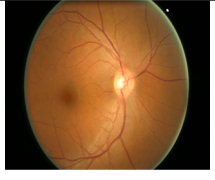
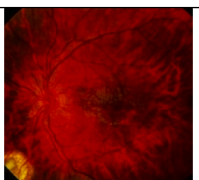
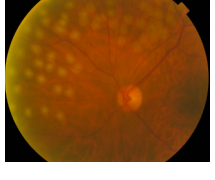
Image classes	Sample images	Image classes	Sample images
Dataset-1		Dataset-2	
“Extreme RB”		Normal	
“No RB”		Background Diabetic Retinopathy	
“Proliferate RB”		Cataract	
“Substantial RB”		Glaucoma	
		Drusen	
“Weak RB”		Maculopathy	
		Choroidal Neovascularization	

Fig. 3. Sample images from experimental dataset-1 and dataset-2.

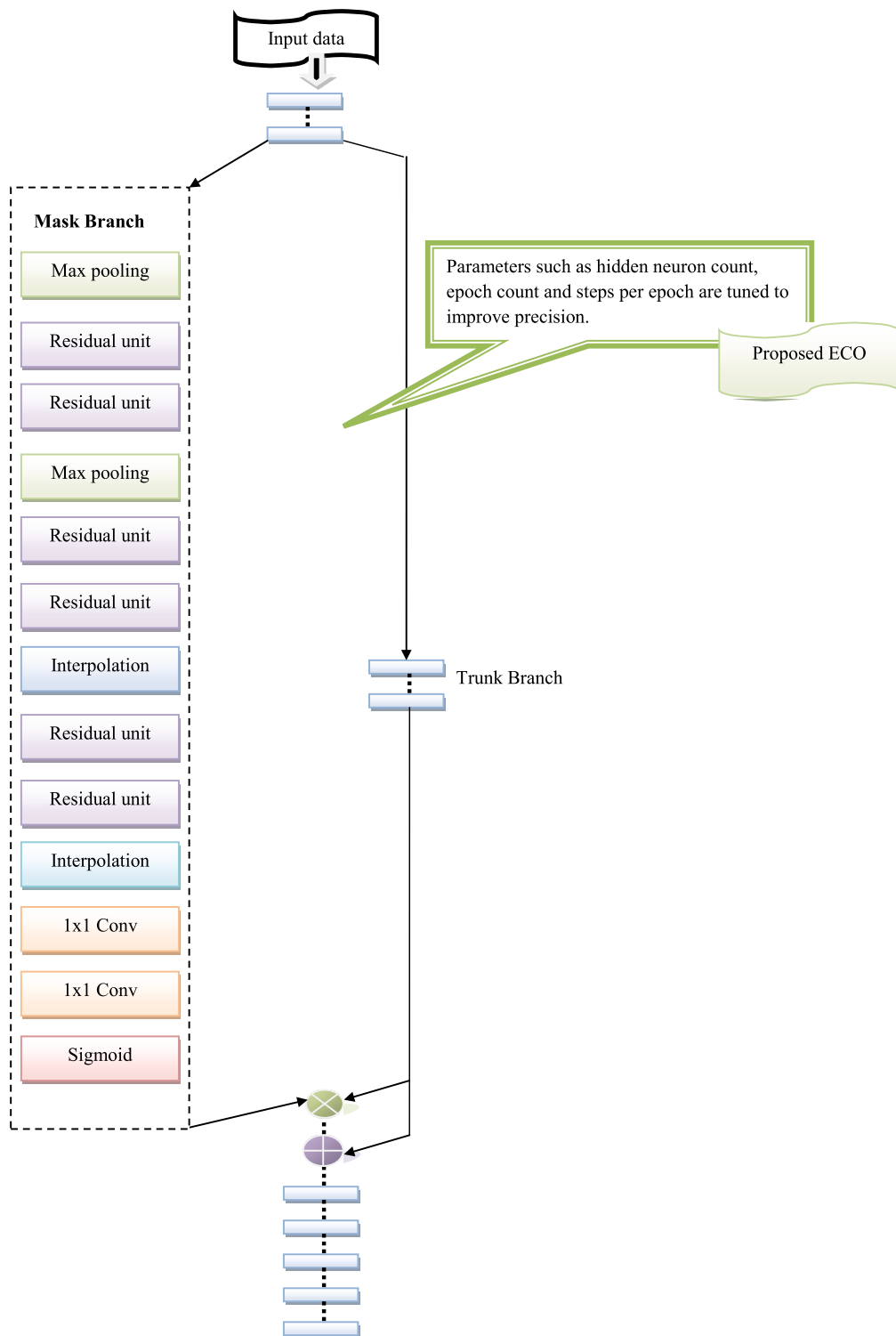


Fig. 4. Structural representation of RAN.

derived from Eq. (11).

$$N_{r,e}(i) = M_{r,e}(i)^* T_{r,e}(i) \quad (11)$$

From Eq. (11), the term r is ranged among all spatial positions and $e \in \{1, \dots, E\}$ denotes channel indexes. Here, the term $M_{r,e}(i)$ indicates the mask size and $T_{r,e}(i)$ shows the trunk branch outcome of the respective input. The entire network is trained using an end-to-end approach.

An attention mask is used to select features during forward inference

and to update the gradient filter during backpropagation. The gradient representation ∂ of the mask for the input feature in the soft mask branch is determined by Eq. (12).

$$\frac{\partial M(i, \lambda) T(i, \mu)}{\partial \mu} = M(i, \lambda) \frac{\partial T(i, \mu)}{\partial \mu} \quad (12)$$

The phrase μ represents the parameters in the trunk branch and the phrase λ indicates the mask branch parameters. Additionally, the result for trunk branch is denoted by $T(i, \mu)$ for the input data i and $M(i, \lambda)$

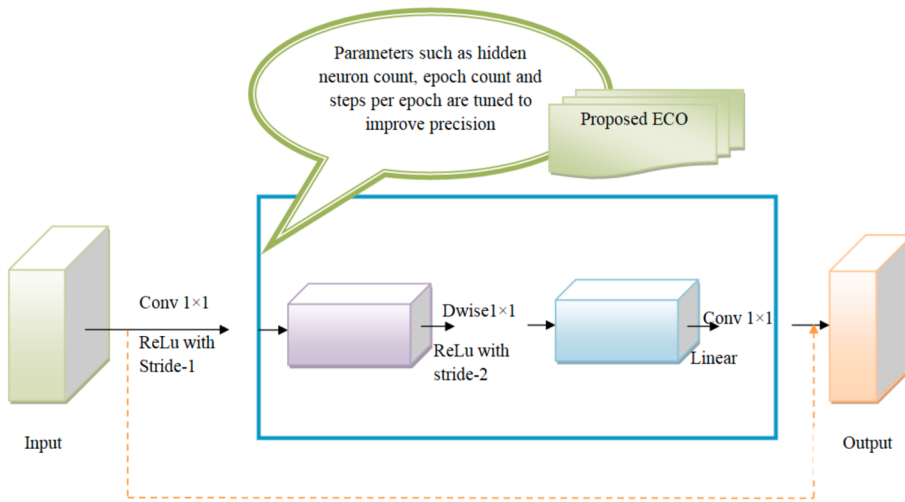


Fig. 5. Architectural view of MobileNetV2.

indicates the mask size. The gradient feature strengthens the attention modules to be resilient in noisy labeling. Masking branches the false labels to update the trunk branch parameters. **Fig. 4** illustrates the structural depiction of the RAN.

The channel attention mechanism is integrated in the RAN technique whereas the attention mechanism is used in a highly dense framework. In **Fig. 4**, the features get extracted using the trunk branch whereas the bottom-up and top-down hierarchy structures are used for learning the different masks. However, the residual modules have achieved good outcomes, but it had lesser computational efficiency and defective diagnosis. Therefore in the RAN model, we optimized the parameters to address the existing issues and enhance the accuracy using the developed ECO. Moreover, the attention modules function not only as the feature selector but can be effectively performed in the updation of the gradient filtering during backpropagation. Only the features in the RAN are selected at once whereas it effectively performs to eliminate the unwanted background in the images. Feature fusion is the process of combining the residual units whereas through the skip connections, the mapping features were identified in the RAN network model. Moreover, the attention mechanism is incorporated using residual units in eye cancer detection. With the help of the attention head, the RAN helps to learn the deep features for providing better detection for eye cancer detection. Henceforth, the residual blocks in RAN comprise 3×3 convolutional layers. The batch normalization and ReLU activation functions are then applied to each layer. As a result, the RAN is implemented using the convolutional layer, max pooling layer and ReLU activation function.

- **Convolutional layers:** The convolution layer in RAN aids in effectively extracting the feature. Here, the convolutional kernel is used to downsample the information to reduce the computation time. The RAN's convolutional layers have been modified to incorporate four convolutional layers, each containing a 3×3 convolutional kernel. For each two blocks, the 1×1 convolutional layers were applied in the RAN network structures. When combined with the residual networks after convolutional operation, the information contained in the image is retained.

- **Max-pooling layers:** It is used for enhancing the receptive field in smaller residual units. Here, the masking branch is attached to the max-pooling layers within the input size of 56×56 , 28×28 and 14×14 respectively. However, to improve the system's performance, the max-pooling layers lower the dimensionality of feature space and the total number of training parameters.

- **Activation function:** The following is a discussion of the activation functions validation for the RAN model comprising ELU, SELU,

ReLU, Softmax and Linear. 90 % accuracy is achieved when the developed method is validated using the ELU activation function. As a result, the SELU achieved 94.5 %, while the ReLU obtained 95 %. With Softmax and Linear activation functions, the resulting accuracy rates are 90 % and 94 %, respectively. Enhanced accuracy is obtained when the proposed approach is validated with the ReLU activation function. Owing to this reason, the ReLU activation function for the RAN model is chosen for this work.

The ReLU activation function plays a crucial role in the residual attention network for eye tumor detection. It aids in introducing non-linearity, allowing the network to identify complex relationships between the tumor detection process and the input data. By applying the activation function, the network becomes more effective and can learn intricate patterns that may indicate the presence of tumors. This improves the network's capability to make accurate detection and improves the overall performance of the eye tumor detection system.

4.3. MobileNetV2

One of the most effective deep learning frameworks is MobileNetV2 [48], which were designed to perform well in a resource-limited environment. The model includes an improved bottleneck layer and inverse residual block. In MobileNetV2, the inverse residual block represents the interface among the thin blocks that differ from a normal residual connection and it is used to connect two expanded units such as point-wise convolution and depth-wise convolution units. Higher accuracy is achieved by the machine and deep learning models' appropriate hyperparameter selection. For applications requiring higher precision, the MobileNetV2 model is not suitable since it gives a poor convergence rate. Therefore, the hyperparameters optimization process optimizes the hidden neuron count, epoch count and step per epoch to provide more rate of convergence. The hidden neurons are present within the range of [5, 255], epoch count of [5, 50], steps per epoch of [50, 250]. Furthermore, the ReLU activation function is employed in the MobileNetV2 framework to overcome the problem of gradient vanishing and also it can learn the complex relationship of the network structures, which means that the network can comprehend and capture the intricate connections between different components of the network. The network's overall functionality can be enhanced by identifying the relationships between each component and its specific functions. This comprehension enables the network to perform better in tasks like eye tumor detection and offers more accurate predictions. Here, the Adam optimizer is used in the MobileNetV2 model since it provides faster convergence for more optimal solutions.

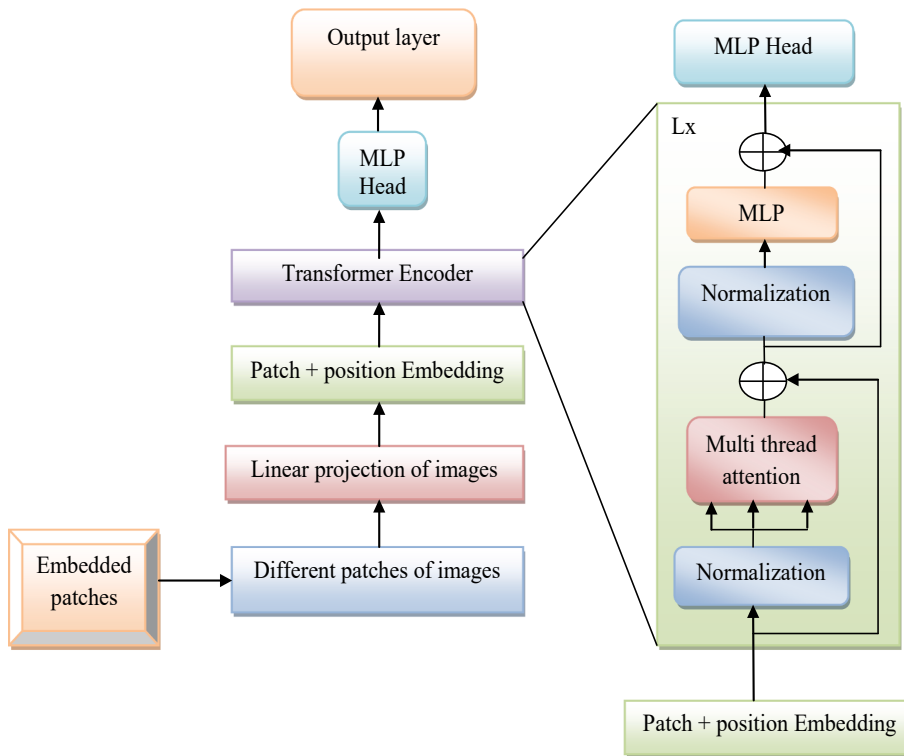


Fig. 6. Architectural representation of vision transformer.

MobileNetV2 is the extended version of MobileNet V1. The width multiplier concept in MobileNet V1 is updated in MobileNetV2 and provides a way to execute the manifold interests (the combination of layer activations) on the pixel at dimension 'D' in a low-dimensional region. Here, the term D represents the channel count. Thus, the width multiplier reduces activation space in the channel till the entire space on the channel is compressed by the manifold interest. In the context of eye tumor detection, this method is enhanced with the aid of ReLU. It is an activation function that plays a role in reducing negative values within the network. The negative values can represent irrelevant or unimportant features. ReLU converts these negative values to zero, which effectively removes the least significant information. This helps the network focus on the important features that can indicate the presence of an eye tumor. ReLU is therefore more useful and aids the network to detect ocular tumors with more accuracy without affecting the performance of the system. This feature uses a width multiplier to combine redundant features to minimize the dimensionality of the data, as this should not have an impact on the detection results in the end. This can be attained by eliminating the input values that generate the negative input for the ReLU activation function. The architectural view of MobileNetV2 is represented in Fig. 5. Fig. 5 indicates the two different blocks of MobileNetV2. At first, the residual block which contains the stride value of 1 in the first layer and also the residual block with stride 2 in the second layer are used for shrinking. The layers such as ReLU6, a point-wise convolution (1×1), depth-wise convolution (filter size 3×3) layers are integrated with the network. Here, the first layer which contains the 1×1 convolution with the activation function of ReLU and also the depth-wise convolution was employed in the second layer. Moreover, the third layer contains 1×1 convolutions with no non-linearity functions.

4.4. Proposed HAN

Eye tumor detection is implemented using the HAN model, which is developed by combining the RAN and MobileNetV2 models to improve the accuracy and efficiency of eye tumor detection. Early diagnosis of

eye tumors is critical in the field of medical imaging because it impacts the effectiveness of treatment and the outcome of patients. The RAN model allows the network to focus on the appropriate regions of the eye images. To achieve it, recurrent attention mechanisms are used to dynamically select informative regions. MobileNetV2 is a lightweight CNN architecture that is specifically designed for mobile and embedded devices. It effectively captures important features and preserves computational efficiency. Yet, the RAN model possesses high computational complexity which is not suitable for certain specific tasks and also it automatically learns the different data patterns in the complex data structures which is prone to overfitting issues. Moreover, the MobileNetV2 model was not suitable for higher precision applications which provide a poorer convergence rate. Due to these issues, the RAN and MobileNetV2 models were integrated to develop the new HAN model. The issues in the RAN and MobileNetV2 can be addressed by parameter optimization that includes "hidden neuron count, epoch count and step per epoch" in RAN and MobileNetV2. Then, the developed HAN model addresses the existing challenge by incorporating attention mechanisms and the feature extraction capabilities of MobileNetV2. The model can focus on areas that possess a higher probability of having features associated with tumors because of this attention mechanism. By emphasizing these areas, the HAN model may more efficiently extract important information and improve tumor detection accuracy.

Conversely, the MobileNetV2 component of the HAN model strengthens its powerful feature extraction capabilities. By combining MobileNetV2 with the attention mechanisms of RAN, the HAN model can efficiently extract and process features from eye images leading to accurate tumor detection. The fusion of RAN and MobileNetV2 in the HAN model creates an optimal effect, whereas the attention mechanisms help the model focus on relevant regions, while MobileNetV2 efficiently extracts and processes features from those regions. This combination enhances the model's capability to detect eye tumors with high precision and recall. The HAN model's performance is further improved through training on large-scale datasets of annotated eye images. This allows the model to learn from a diverse range of tumor patterns and variations, making it more robust and capable of generalizing well to unseen data.

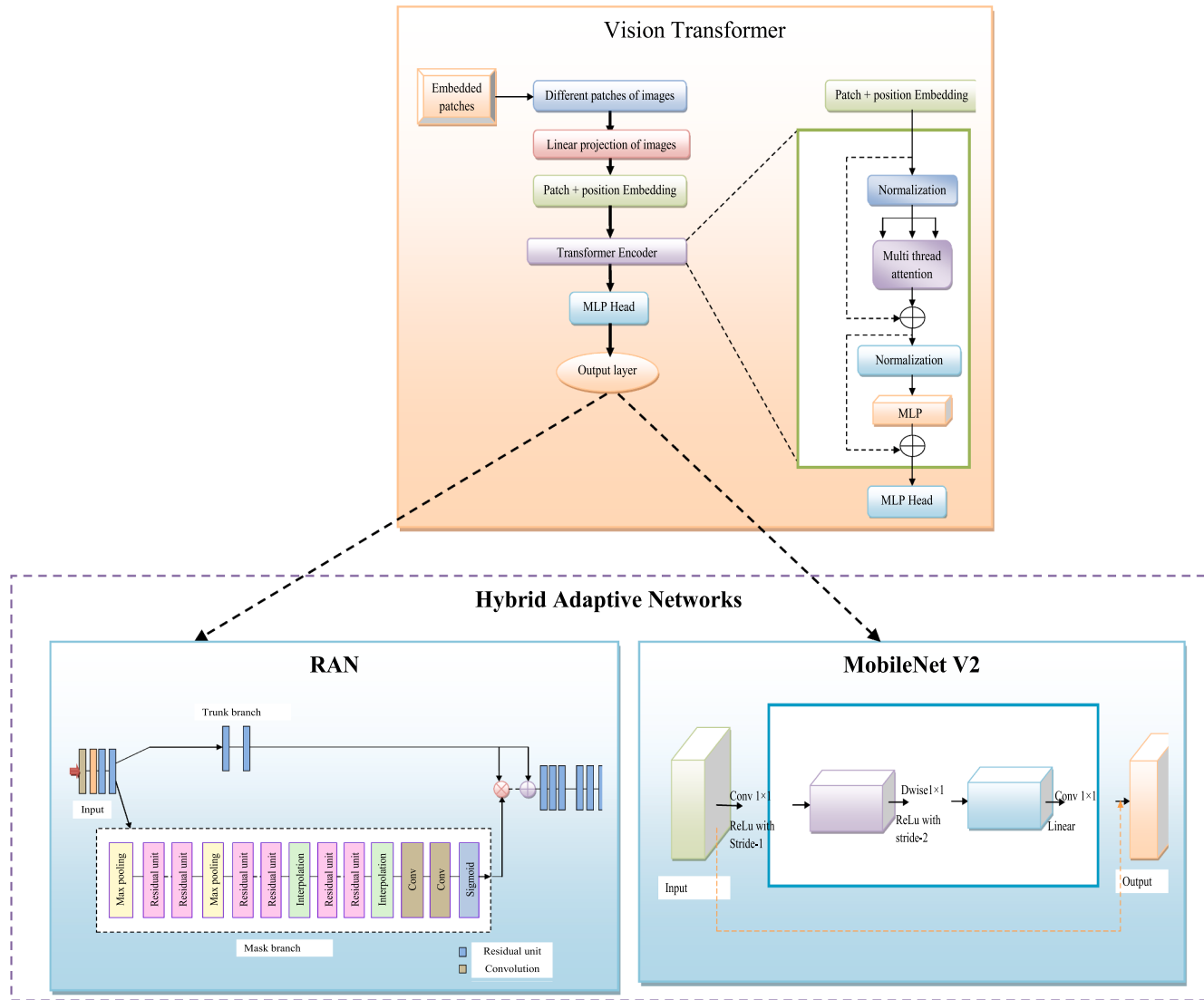


Fig. 7. Systematic illustration of fusing vision transformer logic on HAN.

Finally, the developed HAN model represents a powerful approach to eye tumor detection by incorporating attention mechanisms along with efficient feature extraction and it achieves high accuracy while maintaining computational efficiency. This advancement in medical imaging technology holds great promise for early detection and improved treatment outcomes in the field of eye tumor diagnosis.

5. Integrating vision transformer logic on hybrid adaptive network

5.1. Vision transformer

In comparison to a Vision Transformer, CNNs exhibit higher image-specific inductive bias [49]. In CNNs, two-dimensional neighborhood texture and translation balance are integrated into each layer across the model. In the ViT network, the self-attention layers are global and Multi-Layer Perceptron (MLP) layers provide local equality and translational invariance. The two-dimensional neighbor systems are rarely used at the time of fine-tuning for adjusting the position of the images from different resolutions and dividing the images into patches during the model's early stages. At the time of initialization, the position embedding doesn't contain any details about the 2D position of the divided patches and the structural relationship between the patches. The input images are

initially split into patches. Then, the patches are transformed into lower-dimensional linear embeddings. Next, positional embeddings are added. Finally, a standard transformer encoder receives the sequence as an input. Subsequently, the encoder layer obtains normalized input, which is then given to the multi-headed attention alternating layers. The features are given into the MLP layer after being normalized. Finally, the output layer receives the outcome from the MLP head layer.

In the ViT architecture, “Lx” refers to the different layers in the model. The “L” stands for “layer” and “x” represents the number of specific layers. Each layer in the ViT consists of multiple self-attention and feed-forward sub-layers. These layers help the model learn and extract significant features associated with the input pictures. The necessity of providing “Lx” in the Vision Transformer model lies in the fact that different layers have different functions and contribute to the model's learning process. They help capture and transform visual information at various levels of abstraction. By assessing the behavior and outputs of specific layers, physicians can gain insights into how the model extracts and refines features throughout the network, as well as how it handles input data.

The epoch size and batch size employed to train the network are the hyperparameters of the ViT model. Moreover, the input parameters of

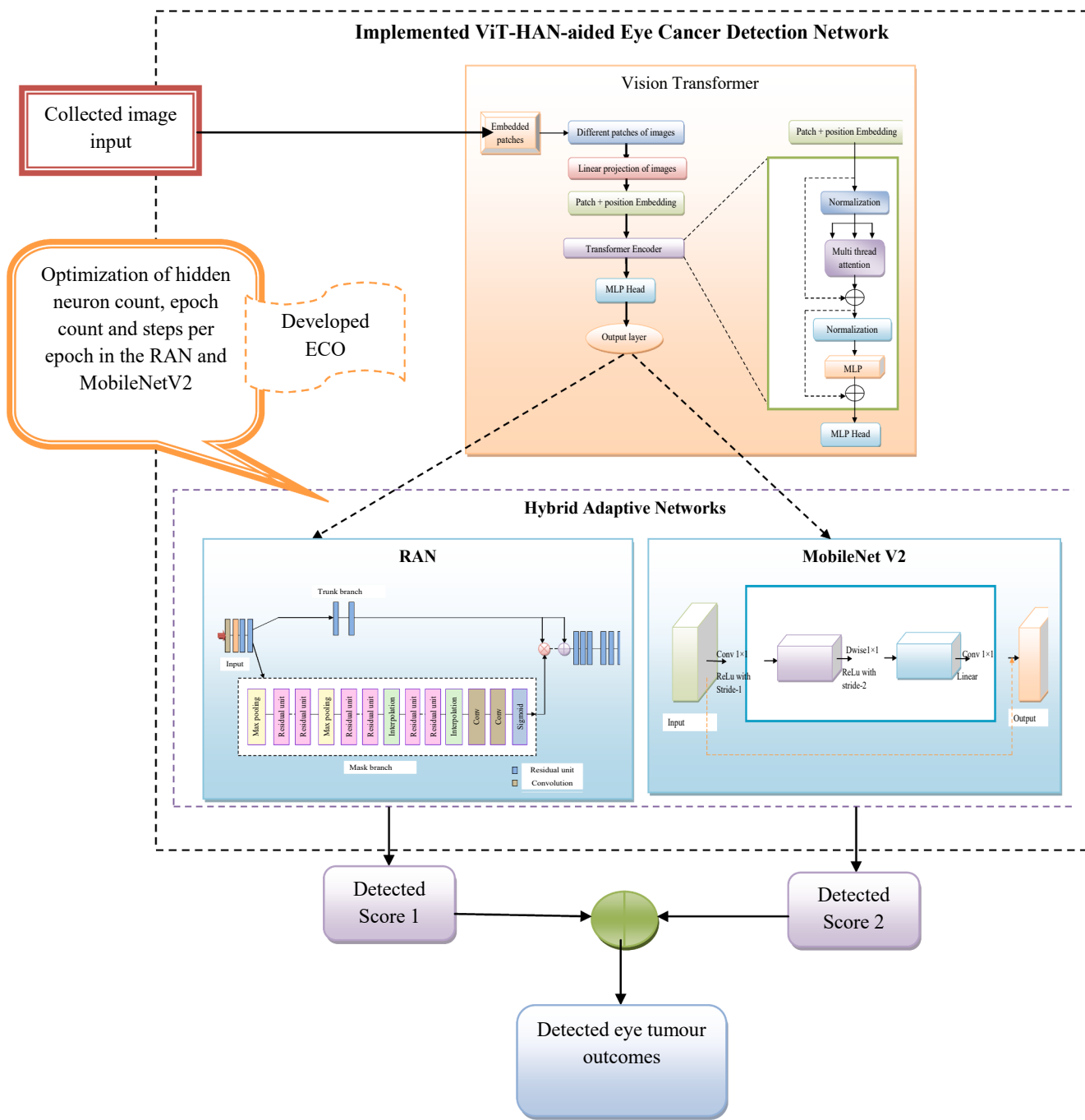


Fig. 8. Structural representation of implemented ViT-HAN-aided eye cancer detection network.

the image detection parameters such as output_attentions, pixel_values, output_hidden_states, head_mask and labels are considered in this research work. In general, the selection of hyperparameters plays a significant role in the deep learning approaches which helps to minimize the training errors. The hyperparameters of the ViT model are crucial and used for attaining efficient performance to eliminate noisy data. Also, the softmax activation function is present in the ViT model, where it contains the smooth gradient to train the model effectively. Moreover, the epoch size and batch size of the ViT model are present in the range of [5, 255] and [4, 128]. The architectural representation of the vision transformer is represented in Fig. 6.

5.2. Fusing vision transformer logic on HAN

The obtained images are given as input into the ViT model. ViT is employed to analyze the images by dividing them into patches. It effectively represents the relationship between the image patches by using self-attention methods which are better than convolutional methods and give better results in image detection tasks that are performed using computerized vision. ViT is commonly used in image segmentation and detection. It is also applied to generative modeling and multi-model tasks like visual reasoning, visual grounding and visual-question answering, etc. It requires few computational resources to train the networks using a huge amount of data. Subsequently, to improve efficiency and yield enhanced results in the detection of ocular tumors, the output features acquired from the ViT framework are

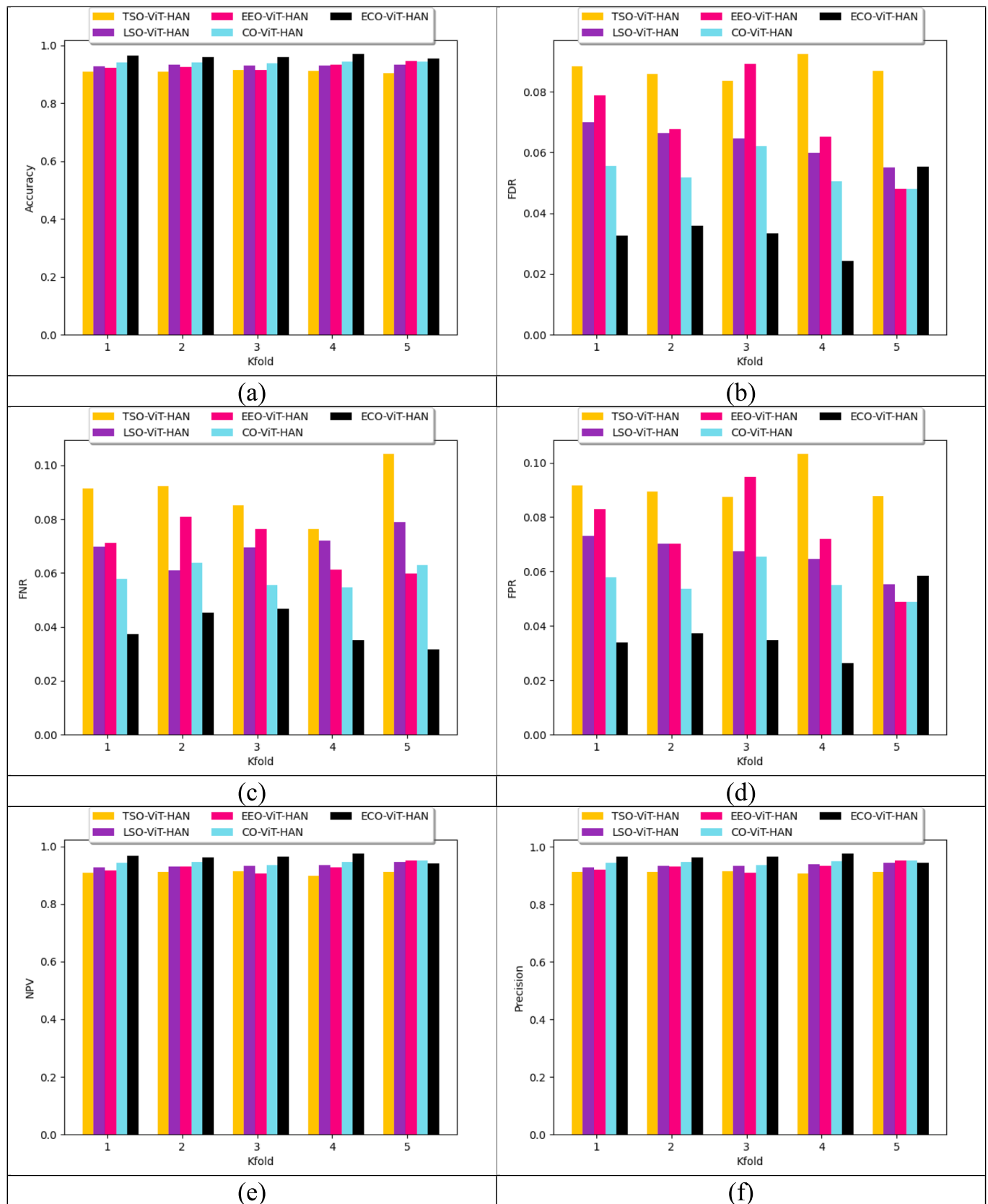


Fig. 9. Performance evaluation of implemented ETDM system using various heuristic approaches: (a) Accuracy, (b) FDR, (c) FNR, (d) FPR, (e) NPV, (f)Precision, (g) Sensitivity, (f) Specificity.

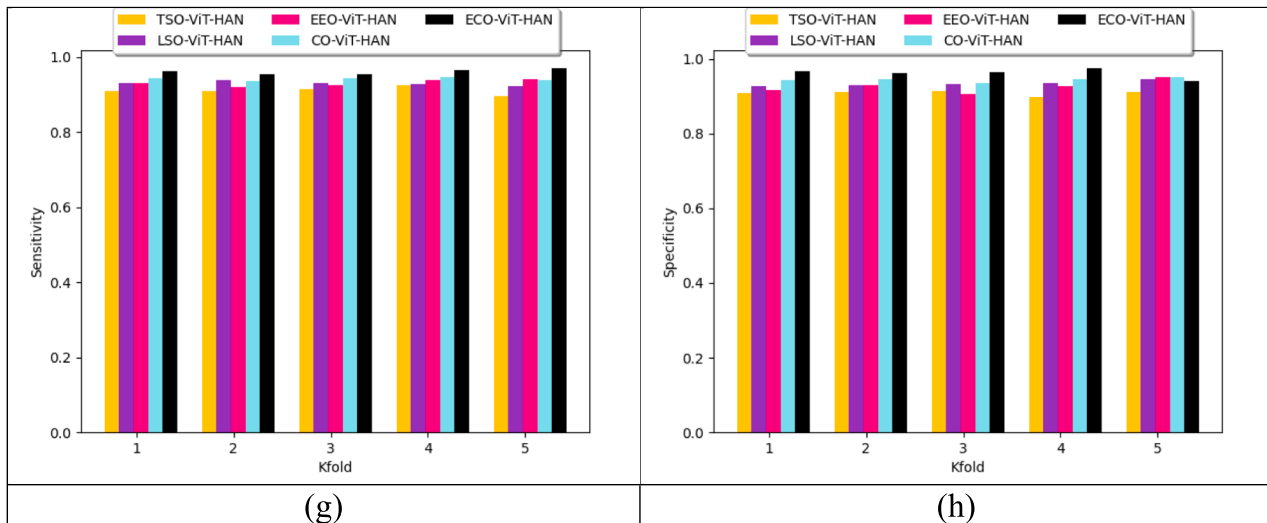


Fig. 9. (continued).

provided as input to the RAN and MobileNetV2. The systematic representation of fusing vision transformer logic on HAN is shown in Fig. 7.

5.3. Implemented ViT-HAN-aided eye cancer detection network

The ViT-HAN-aided model for eye tumor detection is developed using a hybrid network to enhance the system's effectiveness in cancer detection. Early detection of tumors reduces the risk caused by the tumor cells. The parameters from the ViT-HAN are tuned by the implemented ECO algorithm. ViT is fused with the hybrid network to enhance efficiency. In this developed system, ViT is used to focus on the eyeball to detect the tumor cells by fusing with RAN and MobileNetV2 in HAN. In the proposed ViT-HAN-aided eye cancer detection mode, the parameters including “epoch count, hidden neuron count and steps per epoch” in both MobileNetV2 and RAN are tuned to increase the accuracy and decrease the FOR and FPR of the implemented system. The main objectives of the implemented system are given in Eq. (13).

$$\text{Fitness} = \underset{\{HN_x^{RAN}, EC_y^{RAN}, SE_z^{RAN}, HN_a^{MNet}, EC_b^{MNet}, SE_c^{MNet}\}}{\operatorname{argmin}} \left(\frac{1}{\text{Acc}} + \text{FNR} + \text{FPR} \right) \quad (13)$$

From Eq. (13), the expressions HN_a^{MNet} and HN_x^{RAN} denote the “hidden neuron count” of MobileNetV2 and RAN that range between [5, 255]. The terms EC_b^{MNet} and EC_y^{RAN} indicate the “epoch count” of MobileNetV2 and RAN that ranges between [5, 50] and the terms SE_c^{MNet} and SE_z^{RAN} represent “steps per epoch” of MobileNetV2 and RAN that ranges between [50, 250]. ACC is the accuracy and it is described as the proportion of accurate prediction to the total cases.

FNR is the ratio of positives that result in negative test results.

FPR indicates the ratio of true negatives that are incorrectly classified as positives.

The structural representation of the implemented ViT-HAN-aided ETDM is given in Fig. 8.

6. Results and discussions

6.1. Experimental setup

The ETDM system was developed using Python 3.9. The “population size” has been configured to ‘10’ and “chromosome length” to ‘6’ and the “maximum iteration count” is ‘50’. The efficiency of the implemented ECO is evaluated with different heuristic algorithms such as Transient Search Optimization (TSO)-ViT-HAN [50], Lion Swarm Optimization (LSO)-ViT-HAN [51], Equilibrium Optimizer (EEO)-ViT-HAN [52] and

CO-ViT-HAN [45] and techniques like Deep Belief Network (DBN) [53], RAN [44], MobileNetV2 [48] and ViT-HAN [49] are compared and validated for the detection of eye cancer.

6.2. Performance metrics

The efficiency indicators of the developed ETDM considered for evaluation are explained below.

Sensitivity: Sensitivity is defined as the ratio of the true positive rates in the implemented model.

Specificity: It is described as the likelihood of a true negative rate on the implemented model.

Precision: Precision describes the positive predictive value.

FDR: FDR is the expected proportion of false positive rates.

NPV: It is described as the percentage of all negative predictions that are negative.

F1-Score: The F1-Score represents the mean value between precision and recall.

Matthews's correlation coefficient (MCC): MCC is a relationship measure between two binary variables.

6.3. K-fold evaluation of the proposed model using various heuristic approaches

Fig. 9 shows a K-fold-based performance analysis of the developed ETDM employing different heuristic methods. In, Fig. 9(c), the FNR of the developed ECO-ViT-HAN system is 76 %, 62.5 %, 50 % and 51.61 % more effective than TSO-ViT-HAN, LSO-ViT-HAN, EEO-ViT-HAN and CO-ViT-HAN when the “K-fold value is at 5”. Similarly, the performance with other measures is observed to be better for the developed model in all K-fold values. Thus, the proposed ETDM achieves improved performance when compared to other techniques.

6.4. K-fold evaluation of the developed framework based on different classifiers

The performance analysis of ETDM by using various techniques is represented in Fig. 10. In Fig. 10 (c), the FNR of the developed ECO-ViT-HAN is 57 %, 69.2 %, 54.7 % and 46.2 % more effective than DBN, RAN, MobileNetV2 and ViT-HAN when evaluating the K-FOLD value at 3. Thus, this performance has been evaluated to show that the developed system yields superior results when compared to other techniques.

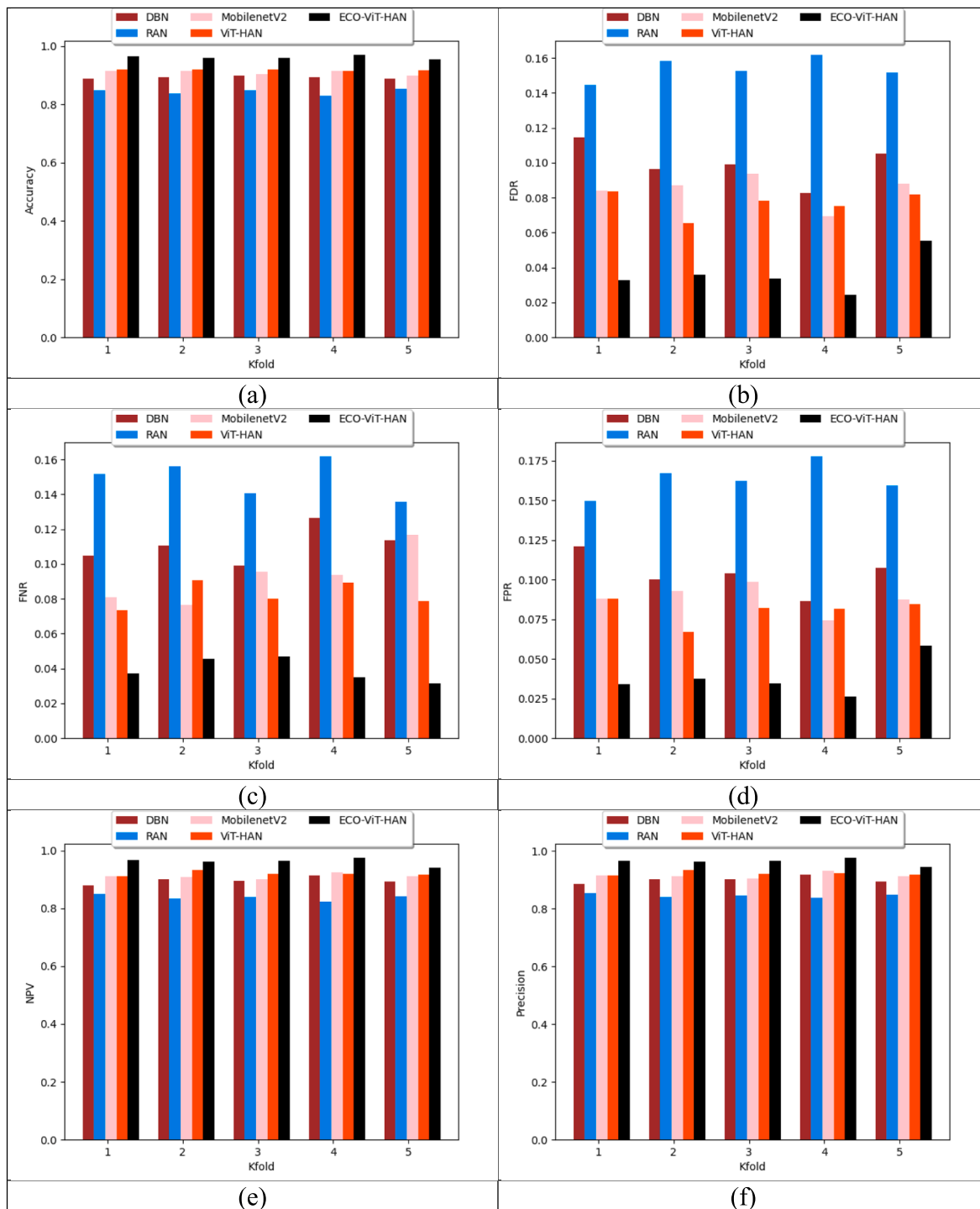


Fig. 10. Performance evaluation of developed ETDM based on different classifiers: (a) Accuracy, (b)FDR, (c)FNR, (d)FPR, (e)NPV, (f)Precision, (g) Sensitivity, (f)Specificity.

6.5. Convergence analysis on developed ECO-ViT-HAN model

Fig. 11 shows the convergence analysis of ETDM. Hence, this evaluation shows that the developed eye cancer detection method is more advanced than other techniques like TSO-ViT-HAN, LSO-ViT-HAN EEO-ViT-HAN, and CO-ViT-HAN.

6.6. ROC analysis on the developed model

The ROC analysis for ETDM is described in Fig. 12. Based on the ROC analysis outcome, the proposed ETDM produces better performance than other techniques.

6.7. Statistical evaluation of the developed model

Table 2 presents an overall statistical evaluation of the eye tumor

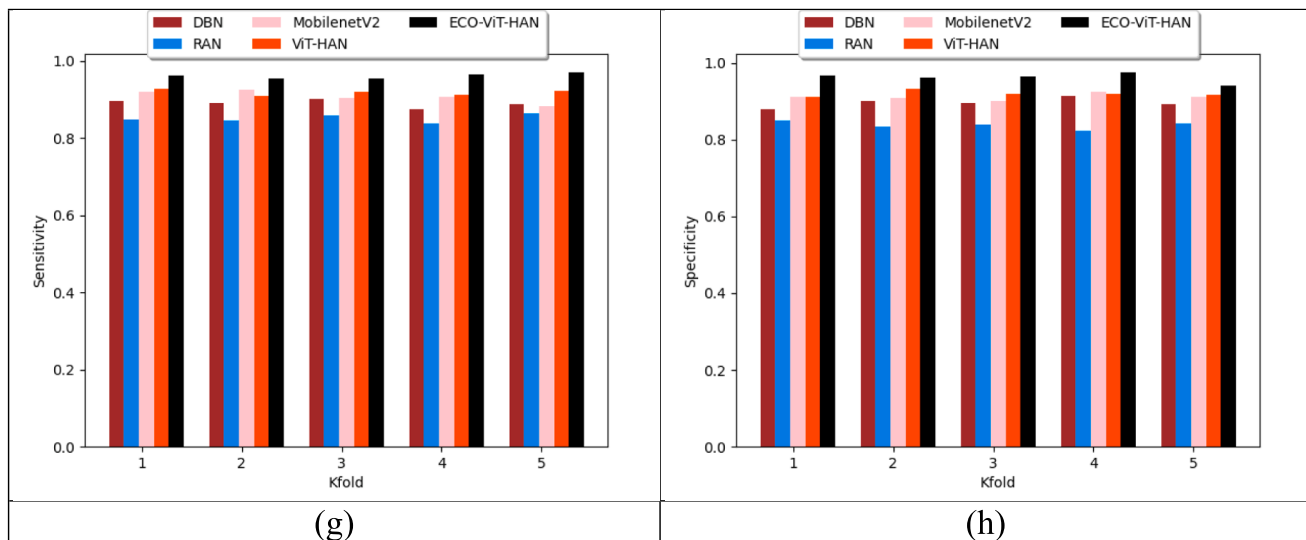


Fig. 10. (continued).

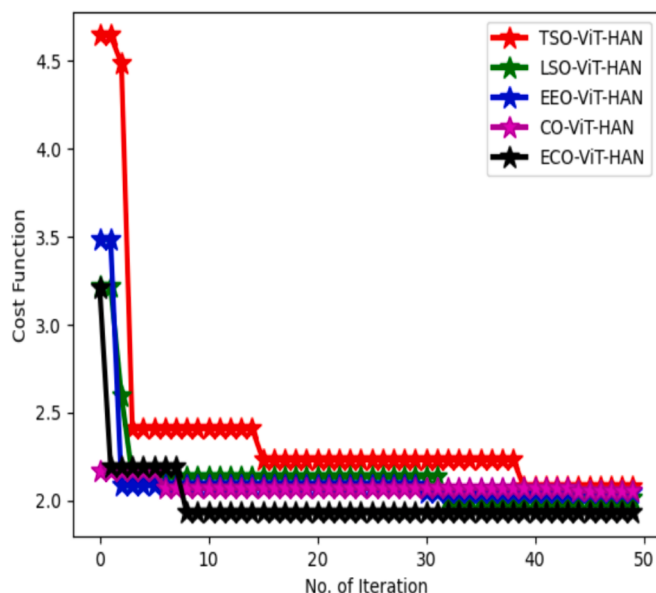


Fig. 11. Convergence analysis on developed ETDM using various heuristic techniques.

detection network. The statistical analysis is performed on the Python 3.9 platform. Several measurements are employed in statistical analysis, including best, worst, mean, median, and standard deviation. Table 2 shows that the implemented model in dataset 1 outperforms TSO-ViT-HAN by 41.19 %, LSO-ViT-HAN by 45.16 %, EEO-ViT-HAN by 43.33 %, and CO-ViT-HAN by 42.61 %, respectively. Thus, the proposed model shows better statistical analysis compared to various models.

6.8. Overall performance evaluation of the proposed model using various methods

Table 3 shows the performance evaluation of ETDM. Here, the analysis is performed using several performance measures to enhance the system's performance. In Table 3, the dataset-1 based on FNR of the proposed system is 2.04 % whereas the existing TSO-ViT-HAN algorithm obtains 10.20 %. The higher value of FNR indicates a decreasing performance in detecting eye tumors. While considering the accuracy analysis in dataset-1, the developed model provides 97 %. Moreover, the

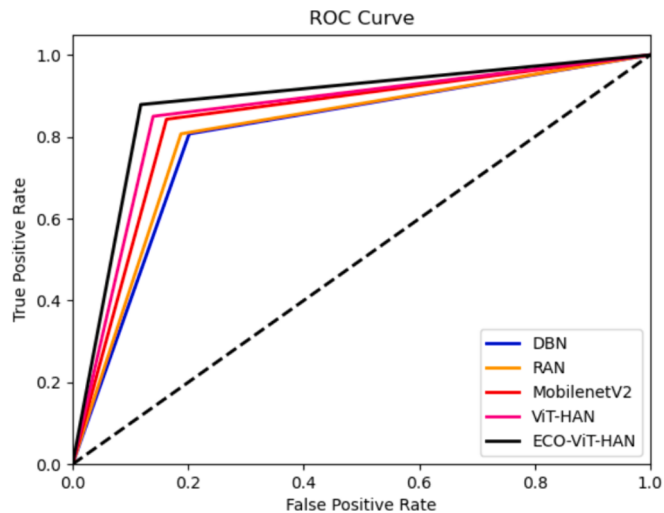


Fig. 12. ROC analysis of developed ETDM using various classifiers.

negative measures like FDR are evaluated using the developed model where the existing TSO-ViT-HAN model shows 26.67 % which degrades the system performance. Here, the performance of the model shows 23.5 %, 27.1 %, 22.7 %, and 10.2 % enhanced than TSO-ViT-HAN, LSO-ViT-HAN, EEO-ViT-HAN, and CO-ViT-HAN in terms of precision analysis. On the other hand, the developed model achieves FDR of 9.43 % for dataset-1 and 12.96 % for dataset-2 showing superiority over the existing approaches. Thus, the proposed eye tumor detection system outperforms other techniques.

6.9. Overall performance evaluation of the proposed model using different classifiers

Table 4 highlights the performance evaluation of ETDM. The performance analysis is performed using various evaluation criteria that include both positive and negative metrics. However, the outcomes of this study would be extremely beneficial in highlighting the accuracy of eye cancer detection. In Table 4, the accuracy of the existing RAN model achieves 83.27 % in dataset-1, where the overfitting could not be resolved effectively. Moreover, the developed model shows 97 % in terms of accuracy analysis using dataset-1 which helps to resolve the issues of overfitting. Similarly, the developed model attains an accuracy

Table 2

Statistical evaluation of the proposed ETDM.

TERMS	TSO-ViT-HAN [50]	LSO-ViT-HAN [51]	EEO-ViT-HAN [52]	CO-ViT-HAN [45]	ECO-ViT-HAN
Standard Deviation	0.5694886	0.236076	0.278731	0.259823	0.1964518
Mean	2.3833725	2.1479997	2.1264581	2.0818948	1.9938867
Worst	4.6441168	4.2169876	3.4883105	3.98043209	3.2111795
Median	2.23413	2.1387176	2.0872702	2.0723028	1.9313547
Best	2.0760457	2.0193021	2.0451359	2.0554779	2.9313547

Table 3

Overall performance evaluation of the proposed ETDM using different heuristic algorithms.

TERMS	TSO-ViT-HAN [50]	LSO-ViT-HAN [51]	EEO-ViT-HAN [52]	CO-ViT-HAN [45]	ECO-ViT-HAN
Dataset-1					
Accuracy	91.43	91.43	91.84	94.69	97.55
Sensitivity	89.80	95.92	91.84	93.88	97.96
Specificity	91.84	90.31	91.84	94.90	97.45
Precision	73.33	71.21	73.77	82.14	90.57
FPR	8.16	9.69	8.16	5.10	2.55
FNR	10.20	4.08	8.16	6.12	2.04
NPV	91.84	90.31	91.84	94.90	97.45
FDR	26.67	28.79	26.23	17.86	9.43
F1-Score	80.73	81.74	81.82	87.62	94.12
MCC	75.93	77.74	77.40	84.57	92.69
Dataset-2					
Accuracy	90.612	91.020	94.286	94.694	96.327
Sensitivity	91.837	91.837	93.878	93.878	95.918
Specificity	90.306	90.816	94.388	94.898	96.429
Precision	70.313	71.429	80.702	82.143	87.037
FPR	9.694	9.184	5.612	5.102	3.571
FNR	8.163	8.163	6.122	6.122	4.082
NPV	90.306	90.816	94.388	94.898	96.429
FDR	29.688	28.571	19.298	17.857	12.963
F1-Score	79.646	80.357	86.792	87.619	91.262
MCC	74.794	75.645	83.560	84.566	89.112

Table 4

Overall performance evaluation of the proposed ETDM using different classifiers.

TERMS	DBN [53]	RAN [44]	MobileNetV2 [48]	ViT-HAN [49]	ECO-ViT-HAN
Dataset-1					
Accuracy	91.84	83.27	91.02	91.84	97.55
Sensitivity	93.88	87.76	93.88	95.92	97.96
Specificity	91.33	82.14	90.31	90.82	97.45
Precision	73.02	55.13	70.77	72.31	90.57
FPR	8.67	17.86	9.69	9.18	2.55
FNR	6.12	12.24	6.12	4.08	2.04
NPV	91.33	82.14	90.31	90.82	97.45
FDR	26.98	44.87	29.23	27.69	9.43
F1-Score	82.14	67.72	80.70	82.46	94.12
MCC	77.98	60.02	76.27	78.58	92.69
Dataset-2					
Accuracy	91.020	83.673	91.429	93.061	96.327
Sensitivity	83.673	85.714	91.837	93.878	95.918
Specificity	92.857	83.163	91.327	92.857	96.429
Precision	74.545	56.000	72.581	76.667	87.037
FPR	7.143	16.837	8.673	7.143	3.571
FNR	16.327	14.286	8.163	6.122	4.082
NPV	92.857	83.163	91.327	92.857	96.429
FDR	25.455	44.000	27.419	23.333	12.963
F1-Score	78.846	67.742	81.081	84.404	91.262
MCC	73.367	59.779	76.513	80.678	89.112

of 96.32 % for dataset-2. Overall, the analysis shows superior performance while analyzing the positive and negative measures. Thus, the proposed ETDM performs better than existing techniques.

7. Limitations of the proposed model

The model's sophisticated architecture combines numerous networks may make it challenging to interpret and understand the specific features or patterns that aid in tumor detection. Additional research may be limited by this lack of interpretability. Moreover, challenging datasets like ORIGA and MESSIDOR are required for the developed model and real-time data collection from tumor-affected individuals is necessary to attain efficient performance in the eye cancer detection framework. Furthermore, the developed model may require significant computational resources and time for training and inference, making it less accessible for resource-constrained environments. The training dataset primarily consists of specific types or stages of ocular tumors and as a result, the model might not be able to accurately detect rare tumor types leading to potential limitations in real-world scenarios. The model may not account for external factors that can influence tumor detection such as patient-specific characteristics, imaging artifacts or variations in imaging methods. These factors can introduce uncertainties and affect the model's performance. Hence, these issues can be resolved in further studies by implementing enhanced deep-learning approaches.

8. Conclusion

The implemented ETDM was developed to detect the cancer cells in the eyeball or interior structure of the eye including the retina, optic nerve, lens, etc. In the initial phase, the images of the eyes affected by tumors were obtained from an online source and then subsequently used to detect tumors. The detection was performed by the developed ECO-ViT-HAN framework comprised of RAN and MobileNetV2 to produce accurate detected results of tumor cells. The parameters in the ECO-ViT-HAN framework have been refined using the proposed ECO algorithm to improve the accuracy and performance of the implemented model. The efficiency of the proposed ETDM was improved by comparing its performance with various classifiers and algorithms. In dataset-1, the developed framework had a 6.7 % higher specificity than DBN, 18.63 % increased than RAN, 7.9 % enhanced than MobileNetV2 and 7.3 % more than ViT-HAN. In dataset-2, the specificity of the developed ECO-ViT-HAN was 3.84 %, 15.95 %, 5.58 % and 3.84 % more than DBN, RAN, MobileNetV2 and ViT-HAN. By considering datasets 1 and 2, the specificity of the developed ECO-ViT-HAN model was 97.45 and 96.429 respectively. This showed that dataset-1 analysis provided more effective results than dataset-2 analysis and it aided in obtaining a broader range of data features, which could be important in developing robust models. Therefore, by using the eye tumor image dataset, the developed ETDM has the potential to achieve a higher detection rate when compared to conventional techniques. It helps detect the tumor at an earlier stage, enhancing the likelihood of effective therapy and superior results. It may also help to minimize the harm to surrounding brain tissues that are healthy and decrease the risk of consequences for patients by offering less-invasive treatment options and reducing costs, providing better outcomes in a shorter period.

CRediT authorship contribution statement

Akshaya B: Writing – original draft, Visualization, Methodology, Formal analysis, Conceptualization. **Sakthivel P:** Validation, Supervision, Conceptualization.

Declaration of competing interest

The authors declare that they have no known competing financial interests or personal relationships that could have appeared to influence the work reported in this paper.

Data availability

Data will be provided upon request.

References

- [1] Y.C. Lin, Y.J. Wang, C.H. Cheng, Y.H. Lin, Contactless monitoring of pulse rate and eye movement for uveal melanoma patients undergoing radiation therapy, *IEEE Trans Instrum. Meas.* 68 (2) (2019) 474–482, <https://doi.org/10.1109/TIM.2018.2846979>.
- [2] G.F. Knoll, L.M. Lieberman, H. Nishiyama, W.H. Beierwaltes, A gamma ray probe for the detection of ocular melanomas, *IEEE Trans. Nucl. Sci.* 19 (1) (1972) 76–80, <https://doi.org/10.1109/TNS.1972.4326488>.
- [3] L. Ichim, D. Popescu, Melanoma detection using an objective system based on multiple connected neural networks, *IEEE Access* 8 (2020) 179189–179202, <https://doi.org/10.1109/ACCESS.2020.3028248>.
- [4] G.A.P. Cirrone, G. Cuttone, P.A. Lojacono, S. Lo Nigro, V. Mongelli, I.V. Patti, G. Privitera, L. Raffa, A 62-MeV proton beam for the treatment of ocular melanoma at Laboratori Nazionali del Sud-INFN, *IEEE Trans. Nucl. Sci.* 51 (3) (2004) 860–865, <https://doi.org/10.1109/TNS.2004.829535>.
- [5] V. Aharonson, V.Y. Coopoo, K.L. Govender, M. Postema, Automatic pupil detection and gaze estimation using the vestibulo-ocular reflex in a low-cost eye-tracking setup, *SAIEE Afr. Res.* 111 (3) (2020) 120–124, <https://doi.org/10.23919/SAIEE.2020.9142605>.
- [6] M.C. Tsui, J.C.H. Cheng, C.P. Lin, Stereotactic radiosurgery for medium and large uveal melanoma with a non-invasive eye immobilization device, a single institutional case series, *J. Formos. Med. Assoc.* (2023), <https://doi.org/10.1016/j.jfma.2023.04.013>.
- [7] I. Bermudez-Castellanos, M.A. Saornil Alvarez, A. Almaraz Gomez, S. Villoria-Diaz, C.G. Alvarez, Impact of COVID-19 on a rare disease (uveal melanoma) in a national reference unit of intraocular tumors in Spain, *Archivos de la Sociedad Espanola de Oftalmologia (English Edition)* 98 (5) (2023) 254–258, <https://doi.org/10.1016/j.oftale.2023.04.007>.
- [8] E.M. Binkley, B.A. King, D.E. Hyer, A. Javed, M.M. Milhem, C.J. Hinz, S.L. Mott, H. C. Boldt, Postoperative echography for optimization of radiation dosimetry in patients with uveal melanoma treated with plaque brachytherapy, *Ophthalmol. Retina* 7 (7) (2023) 620–627, <https://doi.org/10.1016/j.joret.2023.02.010>.
- [9] A.E. Stadhoud, P.M. Puska, T.T. Kivila, Incidence and risk factors for secondary glaucoma in eyes with uveal melanoma, *Ophthalmol. Glaucoma* 6 (1) (2023) 29–41, <https://doi.org/10.1016/j.jogla.2022.08.002>.
- [10] M.C. Gelmi, A.P.A. Wierenga, W.G.M. Kroes, S.G. van Duinen, J.S. Karuntu, M. Marinkovic, J.C. Bleeker, G.P.M. Luyten, T.H.K. Vu, R.M. Verdijk, M.J. Jager, Increased histological tumor pigmentation in uveal melanoma is related to eye color and loss of chromosome 3/BAP1, *Ophthalmol. Sci.* 3 (3) (2023), <https://doi.org/10.1016/j.xops.2023.100297>.
- [11] P. Taherparvar, Z. Fardi, Comparison between dose distribution from 103Pd, 131Cs, and 125I plaques in a real human eye model with different tumor size, *Appl. Radiat. Isot.* 182 (2022), <https://doi.org/10.1016/j.apradiso.2022.110146>.
- [12] C.L. Deufel, S.M.C. Cutsinger, K.S. Corbin, L.A. Dalvin, I.A. Petersen, EyeDose: An open-source tool for using published Monte Carlo results to estimate the radiation dose delivered to the tumor and critical ocular structures for 125I collaborative ocular melanoma study eye plaques, *Brachytherapy* 20 (1) (2021) 189–199, <https://doi.org/10.1016/j.brachy.2020.09.007>.
- [13] M.T. Studenski, N.V. Patel, A. Markoe, J.W. Harbour, S.E. Samuels, Influence of tumor shape and location in eye plaque brachytherapy dosimetry, *Brachytherapy* 19 (2) (2020) 249–254, <https://doi.org/10.1016/j.brachy.2020.01.001>.
- [14] F.S. Rasouli, S.F. Masoudi, S. Keshazare, D. Jette, Effect of elemental compositions on Monte Carlo dose calculations in proton therapy of eye tumors, *Radiat. Phys. Chem.* 117 (2015) 112–119, <https://doi.org/10.1016/j.radphyschem.2015.08.001>.
- [15] W. Zhang, S. Song, H. Wang, Q. Wang, D. Li, S. Zheng, Z. Xu, H. Zhang, J. Wang, J. Sun, In vivo irreversible albumin-binding near-infrared dye conjugate as a naked-eye and fluorescence dual-mode imaging agent for lymph node tumor metastasis diagnosis, *Biomaterials* (2019) 119279, <https://doi.org/10.1016/j.biomaterials.2019.119279>.
- [16] M.L. Zhang, M.J. Suarez, T.M. Bosley, F.J. Rodriguez, Clinicopathological features of peripheral nerve sheath tumors involving the eye and ocular adnexa, *Hum. Pathol.* 63 (2017) 70–78, <https://doi.org/10.1016/j.humpath.2017.02.006>.
- [17] D.G. Marconi, D.G. de Castro, L.M. Reboucas, G.O.B. Gil, R.C. Fogaroli, M.A. C. Maia, M.L.G. Silva, A.C.A. Pellizzon, M.M.M. Chojniak, Tumor control, eye preservation, and visual outcomes of ruthenium plaque brachytherapy for choroidal melanoma, *Brachytherapy* 12 (3) (2013) 235–239, <https://doi.org/10.1016/j.brachy.2012.01.012>.
- [18] J. Huang, S.C. Chan, S.K. GDipPA, V. Lok, L. Zhang, X. Lin, D.E. Lucero-Prisno III, W. Xu, Z.J. Zheng, E. Elcarte, M. Withers, M.C.S. Wong, Disease burden, risk factors, and temporal trends of eye cancer: A global analysis of cancer registries, *Wiley* (2023), <https://doi.org/10.1111/ceo.14353>.
- [19] A.V. Das, P. Kammar, R. Vadapalli, S. Basu, Big data and the eyeSmart electronic medical record system-An 8-year experience from a three-tier eye care network in India, *Ind. J. Ophthalmol.* 68 (3) (2020) 427–432, https://doi.org/10.4103/ijo.IJO_710_19.
- [20] S. Kaliki, A.V. Das, Ocular and periocular tumors in India: an EyeSmart electronic medical record analysis of 9633 cases from a referral center, *Middle East Afr. J. Ophthalmol.* 27 (4) (2020) 199–203, https://doi.org/10.4103/meajo.MEAO_275_19.
- [21] Key Statistics for Eye Cancer Georgia: American Cancer Society, URL: <https://www.cancer.org/cancer/eye-cancer/about/key-statistics.html>.
- [22] J. De Fauw, J.R. Ledsm, B. Romera-Paredes, S. Nikолов, N. Tomasev, S. Blackwell, H. Askham, X. Glorot, B. O'Donoghue, D. Visentin, G. Van Den Driessche, Clinically applicable deep learning for diagnosis and referral in retinal disease, *Nat. Med.* 24 (9) (2018) 1342–1350, <https://doi.org/10.1038/s41591-018-0107-6>.
- [23] Q. Wan, X. Ren, R. Wei, S. Yue, L. Wang, H. Yin, J. Tang, M. Zhang, K. Ma, Y. Deng, Deep learning classification of uveal melanoma based on histopathological images and identification of a novel indicator for prognosis of patients, *Bio. Procedures Online* 25 (1) (2023) 15, <https://doi.org/10.1186/s12575-023-00207-0>.
- [24] R. Ramessur, L. Raja, C.L. Kilduff, S. Kang, J.P. Li, P.B. Thomas, D.A. Sim, Impact and challenges of integrating artificial intelligence and telemedicine into clinical ophthalmology, *Asia-Pacific J. Ophthalmol.* 10 (3) (2021) 317–327, <https://doi.org/10.1097/APO.00000000000000406>.
- [25] A. Maheshwari, P.T. Finger, Cancers of the eye, *Cancer and Metastasis Reviews*, (2018) Dec 15;37:677–90, <https://doi.org/10.1007/s10555-018-9762-9>.
- [26] H. Gu, Y. Guo, L. Gu, A. Wei, S. Xie, Z. Ye, J. Xu, X. Zhou, Y. Lu, X. Liu, J. Hong, Deep learning for identifying corneal diseases from ocular surface slit-lamp photographs, *Sci. Rep.* 10 (1) (2020) 17851, <https://doi.org/10.1038/s41598-020-75027-3>.
- [27] M. El-Abiary, B. Jones, G. Williams, D. Lockington, Fundoscopy screening for intraocular candida in patients with positive blood cultures—is it justified? *Eye* 32 (11) (2018) 1697–1702, <https://doi.org/10.1038/s41433-018-0160-x>.
- [28] R. Neupane, R. Gaudana, S.H. Boddu, Imaging techniques in the diagnosis and management of ocular tumors: prospects and challenges, *The AAPS J.* 20 (6) (2018) 97, <https://doi.org/10.1208/s12248-018-0259-9>.
- [29] P. Rishi, A. Dhami, J. Biswas, Biopsy techniques for intraocular tumors, *Ind. J. Ophthalmol.* 64 (6) (2016) 415–421, <https://doi.org/10.4103/0301-4738.187652>.
- [30] N.M. van Poppel, D.P. de Bruyn, T. Bicer, R. Verdijk, N. Naus, H. Mensink, D. Paridaens, A. de Klein, E. Brosens, E. Kilic, Genetics of ocular melanoma: insights into genetics, inheritance and testing, *Int. J. Mol. Sci.* 22 (1) (2020) 336, <https://doi.org/10.3390/ijms22010336>.
- [31] J. Zhong, T. Huang, M. Qiu, Q. Guan, N. Luo, Y. Deng, A markerless beam's eye view tumor tracking algorithm based on unsupervised deformable registration learning framework of VoxelMorph in medical image with partial data, *Physica Medica* 105 (2023), <https://doi.org/10.1016/j.ejmp.2022.12.002>.
- [32] D.F. Santos-Bustos, B.M. Nguyen, H.E. Espitia, Towards automated eye cancer classification via VGG and ResNet networks using transfer learning, *Eng. Sci. Technol. Int. J.* 35 (2022), <https://doi.org/10.1016/j.jestch.2022.101214>.
- [33] M. Goswami, Deep learning models for benign and malign ocular tumor growth estimation, *Comput. Med. Imaging Graphics* 93 (2021), <https://doi.org/10.1016/j.compmedimag.2021.101986>.
- [34] S.C. Cardoso, O.D. Goncalves, J.V.M. de Sousa, F.M.L. de Souza, D.D. Pereira, Validation of an automatic eye monitoring system for ocular tumors stereotactic radiotherapy, *Radiat. Phys. Chem.* (2020) 108306, <https://doi.org/10.1016/j.radphyschem.2019.04.056>.
- [35] E. Ouabida, A. Essadike, A. Bouzid, Automated segmentation of ophthalmological images by an optical-based approach for early detection of eye tumor growing, *Physica Medica* 48 (2018) 37–46, <https://doi.org/10.1016/j.ejmp.2018.03.014>.
- [36] K. Dimililer, Y.K. Ever, H. Ratemi, Intelligent eye tumor detection system, *Procedia Comput. Sci.* 102 (2016) 325–332, <https://doi.org/10.1016/j.procs.2016.09.408>.
- [37] E.H. Ooi, W.T. Ang, E.Y.K. Ng, A boundary element model for investigating the effects of eye tumor on the temperature distribution inside the human eye, *Comput. Biol. Med.* 39 (8) (2009) 667–677, <https://doi.org/10.1016/j.combiomed.2009.04.010>.
- [38] H. Kunz, C. Derz, T. Tolxdorff, J. Bernarding, Feature extraction and supervised classification of MR images to support proton radiation therapy of eye tumors, *Comput. Methods Programs Biomed.* 73 (3) (2004) 195–202, [https://doi.org/10.1016/S0169-2607\(03\)00074-9](https://doi.org/10.1016/S0169-2607(03)00074-9).
- [39] D.F. Santos-Bustos, B.M. Nguyen, H.E. Espitia, Towards automated eye cancer classification via VGG and ResNet networks using transfer learning, *Eng. Sci. Technol. Int. J.* 35 (2022), <https://doi.org/10.1016/j.jestch.2022.101214>.
- [40] P. Kumar, D. Suganthi, K. Valarmathi, M.P. Swain, P. Vashistha, D. Buddhi, E. Sey, A multi-thresholding-based discriminative neural classifier for detection of retinoblastoma using CNN models, *BioMed. Res. Int.* (2023), <https://doi.org/10.1155/2024/9760632>.

- [41] M.J. Umer, M. Sharif, M. Raza, S. Kadry, A deep feature fusion and selection-based retinal eye disease detection from oct images, *Expert Systems* 40 (6) (2023) e13232, <https://doi.org/10.1111/exsy.13232>.
- [42] S. Ramaswamy, P. Tamayo, R. Rifkin, T.R. Golub, Multiclass cancer diagnosis using tumor gene expression signatures, *Biol. Sci.* 98 (26) (2001) 15149–15154, <https://doi.org/10.1073/pnas.211566398>.
- [43] J. Amin, M. Sharif, M. Yasmin, S.L. Fernandes, Big data analysis for brain tumor detection: Deep convolutional neural networks, *Future Gener Comput. Syst.* 87 (2018) 290–297, <https://doi.org/10.1016/j.future.2018.04.065>.
- [44] M. Zhu, L. Jiao, F. Liu, S. Yang, J. Wang, Residual spectral-spatial attention network for hyperspectral image classification, *IEEE Trans. Geosci. Remote Sens.* 59 (1) (2021) 449–462, <https://doi.org/10.1109/TGRS.2020.2994057>.
- [45] M.A. Akbari, M. Zare, R. Azizipanah-abarghooee, S. Mirjalili, M. Deriche, The cheetah optimizer: a nature-inspired metaheuristic algorithm for large-scale optimization problems, *Sci. Rep.* 12 (10953) (2022), <https://doi.org/10.1038/s41598-022-14338-z>.
- [46] Automated-Eye-Cancer Detection, URL: <https://github.com/rymshasaeed/Auto-mated-Eye-Cancer-Detection/tree/main/dataset>.
- [47] R.K. Srivastava, K. Greff, J. Schmidhuber, Training very deep networks, *NIPS* (2015), <https://doi.org/10.48550/arXiv.1507.06228>.
- [48] B. Singh, D. Toshniwal, S.K. Allur, Shunt connection: An intelligent skipping of contiguous blocks for optimizing MobileNet-V2, *Neural Networks* 118 (2019) 192–203, <https://doi.org/10.1016/j.neunet.2019.06.006>.
- [49] O. Uparkar, J. Bharti, R.K. Pateriya, R.K. Gupta, A. Sharma, Vision transformer outperforms deep convolutional neural network-based model in classifying X-ray Images, *Procedia Comput. Sci.* 218 (2023) 2338–2349, <https://doi.org/10.1016/j.procs.2023.01.209>.
- [50] G. A. Ghazi, E. A. Al-Ammar, H. M. Hasani and R. A. Turky, Transient Search Optimization Based Fuzzy-PI Controller for MPPT of Standalone PV System, 2022 23rd International Middle East Power Systems Conference (MEPCON), Cairo, Egypt, (2022) 1-5. URL: doi: 10.1109/MEPCON55441.2022.10021781.
- [51] J. Liu, D. Li, Y. Wu, D. Liu, Lion swarm optimization algorithm for comparative study with application to optimal dispatch of cascade hydropower stations, *Appl. Soft Comput.* 87 (2020) 105974, <https://doi.org/10.1016/j.asoc.2019.105974>.
- [52] E.H. Houssein, M.H. Hassan, M.A. Mahdy, S. Kamel, Development and application of equilibrium optimizer for optimal power flow calculation of power system, *Appl. Intell.* 53 (2023) 7232–7253, <https://doi.org/10.1007/s10489-022-03796-7>.
- [53] P.R. Jeyaraj, E.R. Nadar, Deep Boltzmann machine algorithm for accurate medical image analysis for classification of cancerous region, *Cognitive Comput. Syst.* 1 (3) (2019) 85–90, <https://doi.org/10.1049/ccs.2019.0004>.